Summer 2019

Paleomagnetic results from Upper Triassic and Middle Jurassic strata of east-central New Mexico, and implication for North American APWP

Masoud Mirzaei Souzani
Western Washington University, mmsmasoud@gmail.com

Paleomagnetic results from Upper Triassic and Middle Jurassic strata of east-central New Mexico, and implication for North American APWP

By

Masoud Mirzaei Souzani

Accepted in Partial Completion
of the Requirements for the Degree
Master of Science

ADVISORY COMMITTEE

Dr. Bernard A. Housen, Chair

Dr. Russell F. Burmester

Dr. Brady Z. Foreman

GRADUATE SCHOOL

David L. Patrick, Interim Dean

Master's Thesis

In presenting this thesis in partial fulfillment of the requirements for a master's degree at Western Washington University, I grant to Western Washington University the non-exclusive royalty-free right to archive, reproduce, distribute, and display the thesis in any and all forms, including electronic format, via any digital library mechanisms maintained by WWU.

I represent and warrant this is my original work, and does not infringe or violate any rights of others. I warrant that I have obtained written permissions from the owner of any third party copyrighted material included in these files.

I acknowledge that I retain ownership rights to the copyright of this work, including but not limited to the right to use all or part of this work in future works, such as articles or books.

Library users are granted permission for individual, research and non-commercial reproduction of this work for educational purposes only. Any further digital posting of this document requires specific permission from the author.

Any copying or publication of this thesis for commercial purposes, or for financial gain, is not allowed without my written permission.

Masoud Mirzaei Souzani

August 28, 2019

Paleomagnetic results from Upper Triassic and Middle Jurassic strata of east-central New Mexico, and implication for North American APWP

A Thesis
Presented to
The Faculty of
Western Washington University

In Partial Fulfillment
Of the Requirements for the Degree
Master of Science

by
Masoud Mirzaei Souzani
August 2019

Abstract

Two contradictory apparent polar wander paths (APWPs) of North America (NA) for most of Jurassic time have been the subject of many studies since the 1990s, and are important to rectify if in order to constrain the tectonic evolution of the continent. Among various efforts to resolve this persistent issue, additional results from well-dated kimberlite volcanics have been used to support a higher-latitude APWP (Kent et al., 2015), and the controversy was blamed on inclination error (IE) in paleomagnetic results of sedimentary units, most of which are from the U.S. South Western interior. Those paleomagnetic poles define the other, lower-latitude path (Kent and Irving, 2010).

Here we present paleomagnetic results from Upper Triassic (Garita Creek, Trujillo, and Redonda Formations) and Middle Jurassic (Entrada, Summerville, and Lower Morrison Formations) sedimentary units of east-central New Mexico, which have magnetostratigraphy that can be correlated with geomagnetic polarity time scales (GPTSs). Positive reversal and fold tests confirm the primary magnetization in these units, which is mostly carried by detrital hematite. Interpretation of noisy and non-linear demagnetization paths, especially ones from Middle Jurassic units, was facilitated by a smoothing scheme, which did not bias the line and great circle fits. The less-than-ideal quality of the Middle Jurassic data could be due to the high rate of polarity reversals for this time period. As a side effect, the frequent usage of the great-circle fits to demagnetization paths was inevitable. We used the sample-level directions from the line fits to estimate the IE using the elongation/inclination (E/I) method of Tauxe and Kent (2004). IE for the Upper Triassic units is negligible because mean directions are horizontal. IE estimated for the Middle Jurassic units is ~20°, however with large 95% confidence limits.

Paleomagnetic poles for Trujillo, Redonda, Summerville, and Lower Morrison Formations of east-central New Mexico, even with IE-correction streak approximately along the 60° parallel (in present coordinates) for most of the Jurassic time, which validates the lower-latitude APWP.

Regardless of the robustness of E/I results, the effects of different amounts of IE can be simply simulated. From existing ca. 163 Ma Summerville Formation paleomagnetic poles, new ones were simulated assuming a possible range of IE. These results show that no amount of the IE correction to the sedimentary results would produce poles consistent with the high-latitude APWP so some other explanation for the discrepancy is required.

Acknowledgements

This project was funded by GSA Research Grant (2017), Geology Department of Western Washington University Advance for Research, and Western Washington University Office of Research and Sponsored Programs.

I am thankful to Russell Burmester, my thesis advisor, for his continuous mentorship and guidance throughout the whole project, even during his valuable retirement times. His welcoming, supportive, and constructive attitude to new ideas and methods are those that I am grateful for. His kind teachings and supports make him more than an advisor to me, like a mentor, a good friend. I am super grateful to Bernie Housen, my thesis supervisor and committee chair, for his supports and helps throughout my whole master's program in WWU. His supports were so certain, that made completion of this program possible for me, with all its hardships and obstacles. I thank Brady Foreman, my thesis advisor, for his quick and valuable feedbacks and responses. My friend, William Callebert, is thanked for his assistance with paleomagnetic sampling under the extreme heat of New Mexico's Summer. Kate Zeigler is thanked for her guidance in the field to spot desired rock units for sampling, and if it was not for her directions, we might not be able to find new outcrops of Summerville Formation. Spencer G. Lucas is thanked for his guidance to better age-determination of the sampled sections. I kindly thank Elizabeth Clemente, who helped me with preparation of my documents for the application process of my master's program. I thank Kate Blizzard, the geology department administrative service manager, for her assistance in the office works of my graduation. Finally, Ben Paulson is thanked for his logistical supports.

Table of Contents

List of Tables

List of Figures

1. Introduction

The paleomagnetic apparent polar wander path (APWP) for the North American (NA) craton has two proposed, and contradictory, paths for the time interval of ca. 190-120 Ma (e.g., Hagstrum, 1993). Although these different paths have been the subject of much study since the 1990s, the issue persists. Among the current efforts to better define the Jurassic APWP, additional results from well-dated kimberlite-type volcanics have been obtained that are used to support a higher-latitude APWP for North America (Kent and Irving, 2010; Kent et al., 2015). Additionally, the rapid shift in the paleomagnetic pole positions (Kent and Irving, 2010) has been used to propose an episode of true polar wander for this time (Kent et al., 2015). The lack of similar rapid shift and different trajectory of APWP from sedimentary rock units, whose paleomagnetic poles define the other, lower-latitude path have been attributed to the inclination error (IE) (Kent and Irving, 2010). These data are mostly from the South Western interior of the North American craton where geologic formations of the appropriate age crop out extensively. Indeed many researchers used paleomagnetic poles of IE-corrected sedimentary units (e.g., Kent and Irving, 2010) or considered a nominal IE for such units they have used in their APWP compilations (Torsvik et al., 2012). Yet it has not been shown that the NA APWP controversy arise from presumed IE associated with the South Western interior sedimentary poles.

Another complication to these hypotheses is that most of the paleomagnetic poles calculated from the southern Western Interior for this period are from units located on the Colorado Plateau (Beck and Housen, 2003; Besse and Courtillot, 2002), which has been inferred to have rotated with respect to the NA craton (e.g., Bryan and Gordon, 1986). However, the exact timing and the amount of its rotation is still a matter of debate. In order to reduce the effect of the Colorado

Plateau's rotation, herein we targeted sedimentary units of east-central New Mexico, which are located east of the Rio Grande rift, the eastern boundary of the plateau.

The paleomagnetism of Triassic – Jurassic Formations on the Colorado Plateau has been extensively studied (e.g., Bazard and Butler, 1992, 1991; Bazard, 1991; Steiner and Helsley, 1974). However, paleomagnetic results from correlative units farther east, such as in central and eastern parts of the New Mexico, are sparse and mostly from Upper Triassic strata (Molina-Garza et al., 1998, 1996; Reeve and Helsley, 1972; Zeigler and Geissman, 2011), with only limited results from some of the Middle Jurassic units (Steiner, 2003; Steiner et al., 1994). One such unit, the Summerville Formation (~163 Ma), has been shown to preserve remanent magnetization from sedimentation or shortly after deposition (Steiner, 2003). None of these studies sought to evaluate possible effects of inclination error, and for use of methods such as the Elongation/Inclination technique (Tauxe and Kent, 2004), the number of existing directional observations is too small to permit a robust examination of inclination error using these methods. Therefore, this formation was initially targeted for extensive sampling (Fig. 1).

Here we present paleomagnetic results from Upper Triassic and Middle Jurassic formations of east-central New Mexico, which enabled us to propose the magnetostratigraphy and paleomagnetic poles of the studied sections. Moreover, obtaining paleomagnetic directions from the Summerville Formation at two localities with different amounts of tilting (Las Vegas and Mills Canyon [Fig. 1]), allowed us to perform a conclusive fold test about the stability of these magnetization directions. Finally, we will discuss the new Middle Jurassic results in comparison with the previous works and will also show, through simulations, whether IE caused the North American APWP discord.

2. Geology

Depositional environments of the U.S. Western interior were dominantly shallow marine to non-marine in Triassic and Jurassic, therefore shallow marine carbonates, fluvial sandstones and mudrocks, evaporites, and eolianites are dominant lithologies of this region (DeCelles, 2004). In east-central New Mexico, Triassic units encompass the Chinle Group, which begins with trough-crossbedded quartzarenites of the Santa Rosa Formation (Lucas et al., 2001). The overlying Garita Creek Formation is dominated by red-bed mudstones and is overlain by the Trujillo Formation, which consists of trough-crossbedded micaceous litharenites with thin interbeds of red-bed mudstone. Red-bed mudstones of the Bull Canyon Formation rest on top of the Trujillo Formation, and they are overlain by cyclic beds of reddish-brown siltstone and sandstone of the Redonda Formation, the youngest formation of the Chinle Group (Lucas, 1995) (Fig. 2). Disconformably on top of the Redonda Formation, Jurassic units begin with trough-crossbedded yellowish-gray to pale reddish-brown eolian sandstone of the Slick Rock Member of the Entrada Formation (Lucas and Woodward, 2001) (Fig. 2). Dark-gray limestone of the Todilto Formation rests disconformably on the Entrada Formation. The disconformably overlying Summerville Formation has lower and upper parts, which the lower part consists of cyclically bedded sandstone and mudstone, whereas the upper part is mudstone and siltstone (Lucas and Anderson, 1997). Sandstones and conglomerates of the Salt Wash Member of the Morrison Formation disconformably overlie the Summerville Formation (Anderson and Lucas, 1996; Lucas and Anderson, 1998) (Fig. 2).

Most of these lithostratigraphic units are bounded by unconformities (Lucas and Spielmann, 2013) (Fig. 2). Due to the similarity of the lithologies, discontinuity of the unconformities, and existence of local (and some unknown) disconformities (Lucas, 1995; Lucas et al., 1999;

Pipiringos and O'Sullivan, 1978), it was troublesome to determine each unit's exact formation name in the field. Therefore, samples were grouped into sets, which we thought corresponded to the formal units.

2.2 Localities and their sampled sets

Upper Triassic and Middle to Upper Jurassic units were sampled from roadcuts at five localities: **Romeroville Exit** from I-25 (route 84), along I-25 near **Las Vegas (NM)**, on route 104 at **Trujillo Mound** ~50 kilometers to the east of the Las Vegas, farther to the southeast on the same road near **Conchas Lake**, and much farther to the north on route 120 at **Mills Canyon** (Fig. 1). At each locality, sample sets, based on lithology, were named by letters indicating the location (e.g., R for Romeroville Exit, and M for Mills Canyon), followed by another letter referring to stratigraphic position in ascending order. More information about the sampled units is reported in Table 1. There we include unit names used by the workers cited above, but note that refinements or reinterpretations of the local stratigraphy can be applied to the new paleomagnetic data using the detailed sample locations provided.

2.2.1 Romeroville Exit:

Sets RA, RB, and RC , from a 35 m section (including sampling gaps) sampled on the eastern side of the road 84, Romeroville Exit from Interstate-25 (Fig. 1), appear to be from the Garita Creek and Trujillo Formations in the middle of the Chinle Group, and thus late-Triassic (Carnian - Norian) in age (personal communication with Dr. S.G Lucas, 2019).

RA is dominantly red shale and siltstone with fine sandstones interbeds and includes about three meters of maroon, moderately-bedded fine sandstone with thin white bands of crossbedding, and conglomerate lenses at the base. These properties match the lower shale member of the Chinle Formation (now Group) described by Kelley (1972), which later was

raised to formation rank and called Garita Creek Formation by Lucas and Hunt (1989). This set is disconformably (Tr-4 unconformity) overlain by RB & RC sets.

RB and RC: RB set is thin-bedded grayish-tan medium-grain sandstone with a layer of conglomerate at its base. Above are the thick-bedded sandstones of RC set. These are the Cuervo Sandstone member of (Kelley, 1972), which are now called Trujillo Formation of Chinle Group (Lucas, 1995; Lucas and Hunt, 1989).

2.2.2 Las Vegas:

Approximately 200 meters of Jurassic strata are exposed at Romeroville Gap, a roadcut on I-25 near the Las Vegas city (Fig. 1). The section encompasses Todilto, Summerville, and the Morrison Formations (e.g., Lucas and Woodward, 2001). Two sampled sets (LA, and LB) are separated by an interval covered by Quaternary deposits. LA set (~55 m) is dominantly pale-reddish sandstone and siltstone, while LB is grayish-green thin-bedded mudstone. The latter, which resembles the Brushy Basin member of the Morrison Formation and is overlain by Mesa Rica sandstone of the Dakota Group, did not yield interpretable results and was omitted from further analysis.

The first two meters of the LA set consist of dark-green organic-rich limestone of the Todilto Formation (Lucas, 2018; Lucas et al., 1999; Lucas and Woodward, 2001). The limestone set is overlain by ~10 m of red mudstone with interbedded sandstone layers of Summerville Formation (Anderson and Lucas, 1992). Above this, there are ~40 meters of pale-red thick-bedded sandstone with some dark laminae, which was previously assigned to the Salt Wash member of Morrison Formation (Steiner, 2003; Steiner et al., 1994) (shaded-area in Fig. 2). However, further stratigraphic analysis has shown that this sandstone-dominated portion should be included as part of the Upper Summerville Formation because it is homotaxial with the Bluff

sandstone of San Rafael Group (Lucas et al., 1999; Lucas and Woodward, 2001). The LA set is unconformably (J-5) overlain by the Salt Wash Sandstone of Morrison Formation, which consists of yellowish-brown, coarse grain, trough-crossbedded sandstone containing some clay clasts (Lucas et al., 1999) and here is as thin as about 5 m (Lucas, 2018) (Fig. 2).

The Todilto Formation equivalent to the northwest in Utah, the Curtis Formation, contains early Oxfordian ammonites (Imlay, 1980). Considering this and the age of the overlying Morrison Formation, deposition of Summerville Formation is bracketed from early to late Oxfordian time (ca. 163-159 Ma) (Wilcox and Currie, 2008).

2.2.3 Trujillo Mound:

At Trujillo Mound, ~50 km east of Las Vegas city on route 104 (Fig. 1), the road cuts through Mesozoic strata from the Upper Triassic Chinle Group that forms most of the valleys and low-lands to the Cretaceous Dakota sandstone, which makes top mesas around the area. Sampled units are Upper Chinle Group, Redonda Formation (TA and TB sets), Exeter sandstone (TC set), Salt Wash sandstone of the Morrison Formation (TD set), and Mesa Rica sandstone (TE set). The last one did not yield interpretable results so is discarded from further analysis.

TA and TB sets: About two meters of light-gray limestone layers, lying disconformably on underlying strata, make up the TA set (Fig. 3). The silty, bioturbated, and micritic nature of this limestone along with its stratigraphic position are the “Basal Marker Bed” of the Redonda Formation (Hester and Lucas, 2001) (Fig. 3).

Over the basal marker bed, there are ~27 m of red, fine- to medium-grained sandstone and interbedded mudstone and siltstone of TB set. Characteristics such as low-angle trough-cross bedding and bedding thicknesses resemble the “SI” facies of Hester and Lucas (2001) of the

Redonda Formation. The age of Redonda Formation is late-Norian to Rhaetian, determined by correlation of the Apachean land-vertebrate faunachron (LVF) (Lucas and Hunt, 1993), which is pinned by the first appearance of a tetrapod genus "*Redondasaurus*" (ca. 215 Ma) to the standard global chronostratigraphic scale (Lucas, 2010).

TC and TD sets: About seven meters of well-sorted tan sandstones of the TC set unconformably rests on top of the Redonda Formation. Its characteristics match the Slick Rock Eolianites of the Entrada Formation (e.g., Lucas and Woodward, 2001). Exposures of the TC set are traceable all around the escarpments in this area. About 20 meters of thin-bedded mudstone of Summerville Formation overlie the TC set, but was not sampled due to large amount of debris. This mudstone is disconformably overlain by ~10 m of thick-bedded, creamy-white channel sandstone of TD set, which resembles the Salt Wash sandstone of the Morrison Formation.

2.2.4 Conchas Lake:

About 30 km to the southeast from Trujillo mound on route 104, near the Conchas Dam lake, there is another exposure of the Trujillo Formation in the area (Fig. 1) (personal communication with Dr. S.G Lucas). This section consists of ~14 m of creamy-white to yellowish-tan, coarse grain, large trough-crossbedded sandstone of the CB set, which is underlain by about one and half meters of brownish-red mudstone layers of the CA set.

2.2.5 Mills Canyon:

Mills Canyon, carved by the Canadian River, exposes Middle to Upper Jurassic strata (Wanek, 1962) (Fig. 1). Five lithological sets (MA, B, C, D, and E) were sampled in this section. Unfortunately, MD and ME sets did not reveal interpretable results.

MA set: Lowermost set of this section consists of about seven meters of loosely consolidated, coarse grained, pebbly sandstone of Entrada Formation (Exeter Member). Most samples yielded very noisy paleomagnetic results.

MB Set: The MA set is gradationally overlain by about nine meters of freshly exposed alternating pale-red fine sandstone and mudstone. Alabaster nodules are abundant in the sandstone layers. These layers are lenticular and commonly pinch out in the outcrops. These are typical characteristics of the unit formerly known as the Bell Ranch Formation in the area (Wanek, 1962), which has been shown to be the eastern extent of the Summerville Formation of the Colorado Plateau (Lucas et al., 1999; Lucas and Woodward, 2001). Stratigraphy of this section was previously studied by Mankin (1972) who mapped the Morrison Formation immediately over the Entrada Sandstone. The reason is that the Summerville strata were not exposed until road reconstruction in 2011 formed the new roadcuts that uncovered these beds.

MC set: The MB set is overlain by about six meters of pale-gray, coarse grained, and medium-bedded sandstone of the MC set. The lithology matches the Salt Wash sandstone of the Morrison Formation, although the J-5 unconformity of Pipiringos and O'Sullivan (1978), which separates the Summerville Formation from its overlying unit (Fig. 2), was not found.

3. Rock magnetic analysis (methods)

3.1. Demagnetization treatments

The oriented samples were processed in the Pacific Northwest Paleomagnetic Laboratory at the Western Washington University. The 2.5 cm in diameters cores were sliced to specimens 2.2 cm in length. Remanent magnetization was measured with a 2G Enterprise model 755 three-axis DC-SQUID magnetometer in a magnetically shielded room with an internal field of less than 350 nT. Progressive thermal demagnetization was employed to reveal components of Natural Remanent Magnetization (NRM) of specimens using the ASC model TD48 furnace.

A total of 345 specimens, 190 from Upper Triassic and 155 from Middle Jurassic Formations, were demagnetized. Samples that were suspected to have magnetite as their main remanence carrier were demagnetized using alternating field (a.f.) in an ASC demagnetizer (with peak fields up to 200 mT). This was generally ineffective, and at best a large portion of NRM (generally >50%) remained after a.f. demagnetization. At least one specimen per layer was selected for pilot thermal demagnetization with 50°-100°C temperature steps below 500°C, 10°-30°C between 500° and 630° or 650°C, and 3°-10°C above 650°C. After this revealed the general demagnetization behavior of each set, most of the specimens were thermally cleaned at large intervals below 500 °C, 30 °- 40 °C steps up to 600 ° or 630 °C, and very small steps (3°-10°C) for temperatures above 630 °C.

In most samples, it appeared that hematite is the main carrier of the remanence, and unblocking temperature ranges above 650°C were used to reveal the Characteristics Remanent Magnetization (ChRM) component of specimens. The linear behavior of the demagnetization paths (at high unblocking temperature ranges) was dealt with Principal Component Analysis (PCA) of Kirschvink (1980), while the great-circle (GC) fits (McFadden and McElhinny, 1988)

were employed for non-linear paths. To not bias directions by possible high temperature overprints, unanchored line-fits were used for most specimens. For those few specimens whose linear path clearly trended toward the origin line-fits were anchored to the origin. Mean paleomagnetic directions for zones with only line-fits were calculated by Fisher (1953) statistics; for those with combined line and GC fits the method of McFadden and McElhinny (1988)was used. Data analysis was carried out using PuffinPlot v. 1.03 (Lurcock and Wilson, 2012).

3.2 IRM

Isothermal remanent magnetization (IRM) acquisition was measured using a MicroMag 3900 Princeton Measurements Corporation vibrating sample magnetometer (VSM). Most of the samples contained a high-coercivity phase (e.g., goethite and hematite) that did not saturate in the 2.2 T maximum field of the VSM. Remanence on the same samples was measured with DC-SQUID magnetometer after magnetization in higher fields up to around 5.0 T produced with an ASC impulse magnetizer. To combine the IRM measurements from the two methods we overlapped three measurements at 1500, 1850, and 2200 mT. The average differences of these steps were used to adjust the offset results from the impulse magnetizer method.

Assuming that the IRM acquisition curves follows a cumulative log-Gaussian (CLG) function, the curves were decomposed by the method of Kruiver et al. (2001) to identify magnetic mineralogy of samples. For example, magnetite would have a low mean coercivity ($B_{1/2}$) compared to hematite, and a population with broad grain size range would have a larger distribution (DP) than one with a narrow size range.

4. Results

4.1. Data Pre-processing

4.1.1. Averaging (smoothing)

One of the main issues with data interpretation was that demagnetization paths for many specimens were not clearly linear or non-linear due to the high level of noise. This became more problematic at higher temperatures, where signal-to-noise ratio was small during unblocking of most of the ChRM components above ~650 °C. To reduce the visual impact of the noise (Fig. 4), we decided to smooth (average) measurements using a 0.5-1-0.5 weighting scheme. This means that for each treatment step we used the following: [(0.5 × previous measurement) + (the measurement) + (0.5 × the following step)] / 2; and for the last step to be consistent with the rest of the modified steps used (0.5 × previous + last step)/1.5 formula.

Perhaps the major concern with smoothing is that it smears the temperature-moment relationships. However, in practice, the uncertainty of the temperature gradient in the oven (~10°C) would have already disturbed the temperature-moment relationship. To avoid smoothing contributing to the uncertainties, we were reluctant to fit lines (or GCs) on temperature steps that are more than 10°C apart.

To determine the ChRM direction of specimens, lines, or GCs (Fig. 4), were fitted on the smoothed version of data and then the same Tub range and fit type were used on the raw data. The maximum angular deviations (MAD) were generally <10° for the smoothed dataset, while usually larger MADs were observed on the identified components of the raw data (20°-30°). The zone-mean paleomagnetic directions of raw and smoothed datasets are very similar with generally better precision for the smoothed version (see Table 2), which show that the smoothing did not bias the results and was beneficial to identify the ChRMs.

4.1.2. Site Division

Initially, the two or three samples from each sampled horizon were grouped as a site in the hope that each would have sampled the magnetic field at different times. However, because most of the samples showed very noisy results and non-linear demagnetization paths, the best approach seemed to be to group samples from adjacent horizons that preserved a single polarity. Each such group we call a 'zone' (Table 1). Thus, zone-mean directions come from the specimens that appeared to belong to a single chron, or transition/excursion zones.

4.2. Upper Triassic Formations

Upper Triassic units are Garita Creek, Trujillo, and Redonda Formations. Except for the limestone layers of the TA set (Basal Marker Bed [Fig. 3]) of the Redonda Formation, the rest of the Triassic strata are terrigenous rocks. NRM intensities range between 1.24×10^{-4} to 2.96×10^{-2} A/m. Demagnetization behavior of the representative samples of the Upper Triassic units along with either the same or the sister sample's IRM decomposition results (Kruiver et al., 2001) are presented in Fig. 5.

All of the Carnian-Norian (ca. 223 Ma) age Garita Creek and Trujillo Formations' zone-mean directions show a normal polarity magnetization (Fig. 5a-e). However, there is one excursion zone identified at the top of the Conchas Lake section (CB-E1). After removal of a (viscous) low-temperature component from many samples at 150 °-330°C, NRM intensities gradually decrease at middle temperature ranges between 250°- 400°C and 580°- 620°C, which could be due to unblocking of magnetite and/or pigmentary hematite. The stable ChRM components were isolated between 660°C and 685°C.

Paleomagnetic directions of the Redonda Formation (ca. 214 Ma) preserved two polarity reversals. Although the first layer (zone TA-R) of the TA set was discarded from magnetic pole calculations, its magnetization was acquired in a reversed polarity. In TA set, after removal of a low temperature (150°- 200°C) component, the NRMs gradually decay on an almost linear path toward the origin between ~300° and 675°C with a slightly sharp drop after 640°C (Fig. 5f). This is from unblocking hematite with a wide grain size distribution; no low-coercive (< 100 mT) constituent (e.g., magnetite) exists in this set, also confirmed by its IRM decomposition results (Fig. 5f)

In many specimens, the IRM acquisition curves were decomposed into three magnetic phases (Fig. 5). The phase normally with the highest $B_{1/2}$ (mean coercivity), generally > 1000 mT, could be iron oxyhydroxide (e.g., goethite), as there are detectable drops of NRM intensities at 150° - 200°C. The soft fraction ($B_{1/2}$ < 100 mT) contribution to the IRM in the Garita Creek and the Trujillo Formations are between 25 – 40%, while in the Redonda samples it is < 10 % (0 % in the TA set). Generally, the dominant constituent, and likely the remanence carrier, is in the high-coercive fraction. In the Trujillo Formation this dominant phase has an average mean coercivity ($B_{1/2}$) of ~225 mT and dispersion parameter (DP) of ~0.31 mT, whereas in the Redonda Formation the mean $B_{1/2}$ and DP are ~550 and ~0.37 mT, respectively. This may indicate a coarser grain size of the ferromagnetic population in the Trujillo Formation than the Redonda Formation.

Both the remanence decay curves and the IRM decomposition analysis show that the hard fraction is mostly hematite, which in some sets (e.g., CB and TB set [Fig. 5e, g-h]) has distinctively different population of grain sizes. It is likely that pigmentary hematite corresponds to the smaller grain-size population, as their DP values < 0.30 mT also hint for a narrow grain-

size distribution and thus a possible chemical source. Because the unblocking temperature (T_{ub}) range of pigmentary hematite is usually < 500° - 600°C (Jiang et al., 2015), which overlaps with magnetite's T_{ub} range, ChRM components were isolated at higher temperature ranges to avoid contributions from pigmentary hematite and magnetite.

4.3. Middle Jurassic Formations

Sampled Middle Jurassic units are Todilto, Entrada, Summerville, and Morrison Formations (Table 1). There is only one zone in the Todilto Formation. Although it recorded a reverse polarity, its results are not well-defined enough to be included in later analysis. More than 90% of the mid-Jurassic samples have an NRM intensity range between 1.93×10^{-5} and 3.18×10^{-3} A/m. Demagnetization paths of the representative samples of the Middle Jurassic units along with either the same or the sister sample's IRM decomposition results (Kruiver et al., 2001) are presented in Fig. 6.

Slick Rock Sandstone of the Entrada Formation was only sampled at Trujillo Mound section. Paleomagnetic directions from the bottom-most part of this set showed large deviations from the expected dipole direction and because the previous polarity is unknown due to the J-2 unconformity, this part is assigned to an excursion period. The rest of this set preserved a normal polarity (Table 2). The stable ChRM components were isolated between 630°C and > 650°C (Fig. 6h).

The late Carnian-Oxfordian aged (ca. 163 Ma) Summerville Formation was sampled at Mills Canyon and Las Vegas localities (Table 1 and Fig. 1). At both sections, paleomagnetic reversals were recorded. During thermal demagnetization NRM intensities decreased by 10 – 30 % at 350° / 500°C in most of the samples (Fig. 6a-e). A coherent and discernable component was not observed at the expected T_{ub} range of magnetite. In most specimens, a component demagnetized

between ~590° and 660°C was different in direction (usually steeper) from the stable ChRM component with T_{ub} range from 660° to 680°C, which is clearly evident in Fig. 6b. Our inference is that the former could correspond to the pigmentary hematite, while the latter is from detrital hematite.

Only the lower parts of the Morrison Formation were sampled as the focus was on the Summerville Formation. Generally, a (viscous) low temperature component was removed at 350° / 450°C (Fig. 6f-g). The ChRM component started to unblock gradually after 600°/ 620°C, with a sharp drop between 660° - 685°C (Fig. 6f) in some specimens.

The IRM acquisition decomposition analysis revealed three to four magnetic phases (Fig. 6). Although a phase with the $B_{1/2}$ >1000 mT was identified in many samples, it might not be goethite as a significant decrease in NRM intensities around 150°C was not observed. The soft fraction ($B_{1/2}$ < 100 mT) contributions to the IRM in the Entrada and the Summerville Formations are < 20% and in the Morrison Formation is 15 – 30%. The dominant constituent has high mean coercivities in all three Formations. This phase has an average mean coercivities ($B_{1/2}$) of ~345 mT, ~260 m, and ~540 mT in the Entrada, the Summerville, and the Morrison Formations, respectively. Except for the Entrada Formation the dispersion parameter (DP) for all other Formations is >0.30 mT. The differences in the averaged mean coercivities may indicate the differences in the grain size of the corresponding ferromagnetic mineral.

In the Summerville Formation samples, the contribution of a soft fraction to the IRM acquisition curves is small, and it is in agreement with the small decrease of NRM intensities in the T_{ub} range expected for magnetite. However, the soft fraction in the Morrison Formation could be mostly maghemite, because it holds a small but rather a fair share in the IRM but not in the

T_{ub} range of magnetite and their NRM decrease at 350°/ 500°C might be due to the inversion of maghemite (γFe_2O_3) to hematite (αFe_2O_3) (Dunlop and Özdemir, 2001).

Like the Upper Triassic units, both the remanence decay curves and the IRM decomposition analysis of the Middle Jurassic units indicate that the hard fraction is mostly hematite. Also, the main remanence carries may reside in that fraction. In the Summerville Formation It appears that two population of hematite coexist, one with average fine grain size and narrow distribution (~ $B_{1/2}$ = 470 mT / DP = 0.26 mT), and the other coarser with wider distribution (~ $B_{1/2}$ = 260 mT / DP = 0.33 mT) (Fig. 6b and e). The latter could correspond to the detrital hematite, while the former likely is the pigment. Similarly, in the Morrison Formation two distribution of hematite grains are observed, however, although the fine-grain distribution is the dominant component in the IRM, the ChRM components were isolated at high T_{ub} ranges (> 660°C) in agreement with the coarser grain-size distribution (Fig. 6g-h).

The paleomagnetic directional analysis of the sampled Upper Triassic and the Middle Jurassic strata are reported in Table 1. Results are from component fitting on both raw and the smoothed versions of data. The zone-mean directions, calculated from line fits (PCA of Kirschvink (1980)) with MAD < 10° (< 5° for anchored lines), and line fits combined with great-circle fits (McFadden and McElhinny, 1988) with MAD < 10° are presented in the Supplementary table 1 and 2, respectively. For our further analysis and discussions, we preferred to use the smoothed paleomagnetic directional data presented in Table 2. Paleomagnetic mean directions for zones that represents the polarity zones (Table 2) are shown in Fig. 7.

4.4. Stability tests

4.4.1. Fold test

In east-central New Mexico, most of the sedimentary strata have nearly horizontal (dips < 10°) (Johnson, 1974). An exception is near the Romeroville Gap, where uplift of the Sangre de Cristo Mountains during the Laramide orogeny tilted strata ~ 30° – 40° (Skotnicki, 2003). Acquiring enough paleomagnetic mean directions from the Summerville Formation at both flat and tilted regions (Mills Canyon and Las Vegas sections) of this monocline allowed us to examine the stability of the direction through the fold test using the bootstrap technique of Tauxe and Watson (1994).

The test results are shown in Fig. 8. The total number of five zone-mean directions, two from the Mills Canyon and three from the Las Vegas section, were used to perform the parametric bootstrap test. Although the results show tighter clustering in the tilt-corrected coordinates (Fig. 8a), the results of the maximum value of the largest eigenvalue (τ_1) were inconclusive. This issue is probably due to asymmetricity of the fold that raises the chance of failure of the Tauxe and Watson's (1994) test, with small-sized datasets (McFadden, 1998).

To overcome the issue simulated mean directions were calculated for each zone. Such a synthetic datasets were made using each zone's statistical precision parameters, then their mean direction was calculated. The number of iterations to generate synthetic zone-mean directions was equal to the number of directions in each zone. The results of the 10k bootstraps (Fig. 8b-c) indicate a positive fold test as the 95% confidence limits of the degree of untilting to produce the maximum τ_1 are between 73 and 139 % (Fig. 8b). This suggests that the magnetization has acquired before folding.

4.4.2. Reversal test

As several reversals were observed in the Upper Triassic and the Middle Jurassic strata, the reversal test (Tauxe, 2010) was conducted on polarity zone-mean directions. However, there are some shortcomings with the simple bootstrap of Tauxe's (2010) approach, especially when dealing with a small number of paleomagnetic directions in each polarity mode. First, the number of bootstrapped means for each polarity mode will become the same, while the number of mean directions within each mode are not necessarily equal. This will give artificially higher precision to the polarity mode with a smaller number of directions. Second, in the simple bootstrap reversal test the uncertainty of each site-mean direction is not included, which might bias the outcome toward less-precise site means. Therefore, considering only this issue, use of the parametric bootstrap reversal test is advisable even if a large number of site-mean directions exists for each polarity mode. Third, the distribution of site-mean directions is not necessarily Fisherian. This might get more problematic when dealing with data from time periods of rapid APW movement. The final drawback is lack of robustness with the bootstrap when the number of the data is small, usually $\sim< 3$ per polarity mode.

We modified Tauxe's (2010) approach to perform parametric bootstrap, when the number of paleomagnetic mean directions is small in either polarity modes. Another modification is using the direction of the maximum eigenvector of the site-mean distributions in each polarity mode, as the distribution of the site-mean directions is not necessarily Fisherian. To compare the result of the simple (Tauxe, 2010) and parametric bootstrap reversal test proposed here, the results of the combined Summerville and Morrison Formations' zones means (9 zones) are presented in Fig. 9a and c. This show the robustness of the parametric bootstrap reversal test, especially when number of the paleomagnetic directions are small. The parametric bootstrap reversal test result of

the Summerville Formation zone-mean directions is positive, which is consistent with the magnetization being acquired during or shortly after sedimentation.

Moreover, in circumstances that the number of site-means in either polarity modes is <2, synthetic directions can be created based on the statistical precision parameters of each site means. Such a simulation was used to perform the simple bootstrap reversal test on the Upper Triassic zones (the only reverse zone is TB-R). Then, the synthetic population of the sample-level directions was fed to the simple bootstrap reversal test (Tauxe, 2010). The result indicates a positive reversal test for the Upper Triassic directions (Fig. 9d).

4.5. Inclination Error (IE)

Inclination shallowing or inclination error (IE) in sedimentary rocks results from a tendency for anisotropic magnetic particles to rotate toward horizontal relative to the ambient field while or after being deposited (e.g., Jackson et al., 1991). This effect can be quantified with a flattening factor (*f*), using well-known King's (1955) equation (1), where I_C and I_O are true and measured inclinations, respectively:

$$\tan I_O = f \tan I_C \qquad (1)$$

The statistical geomagnetic field models using a great Gaussian process (GGP) (e.g., TK03.GAD (Tauxe and Kent, 2004)) predict the distribution of magnetic directions at different latitudes to be elongated along meridians whereas flattening imparts E-W elongation (Tauxe, 2005). The elongation/inclination (E/I) method of Tauxe and Kent (2004) searches for the *f* value that produces the E/I combination compatible with the geomagnetic field model. One of the assumptions of E/I method is abundant (>150) well-defined magnetic directions that have recorded a statistically meaningful paleosecular variation (PSV) (Tauxe et al., 2008).

The paleomagnetic directions obtained as line fits are too few to apply the standard E/I method for all formations. Use of site or zone mean directions derived from line and GC fits is not ideal for the E/I method because each mean likely averaged a significant portion of the secular variation. However, we used the sample-level directions from the line fits of the Upper Triassic Formations (n=120) and the Summerville and Morrison Formations of the Middle Jurassic units (n=62). Presumably, the paleomagnetic directions of the Upper Triassic and Middle Jurassic Formations were acquired over ca. 10 and 5 Myr time spans, respectively. Results are presented in Fig. 10 and Table 3. To decrease the chance of bias due to the polar wander and to increase the number of directions to satisfy the assumption of E/I method, we combined the sample-level directions of this study's Summerville Formation (34 directions) with Steiner's (2003) Trujillo section (62 directions) (see Fig. 10e-f and Table 3 for the E/I results). Steiner's (2003) directions were not tabulated, and so were digitally obtained from her Figure 4, so some errors might be associated within those directions.

The E/I method results (Table 3) estimate ~19 - 20° inclination error for the Middle Jurassic units, although their bootstrapped 95% confidence limits are large (~25°). Deenen et al. (2011) introduced reliability criteria for paleomagnetic directions, which should be applied for studies that using geomagnetic field models, like TK03.GAD, to assess the IE. The criteria use an N-dependent A95 (95% confidence circles about the paleomagnetic pole) envelope to ascertain that the distribution of the paleomagnetic direction represents only PSV. These criteria applied to the Jurassic data indicate that all A95's exceed the A95max calculated for the corresponding N. This shows that scatter of the Middle Jurassic directions has other source(s) beside PSV. For our data, this additional scatter is likely due to polar wander and not random noise, and probably denotes excessive time spans considered for the analysis.

The directions from Upper Triassic strata have reasonable A95s but despite large *f* (*f*=0.43) IE is negligible because the mean direction is horizontal (I_O = 0.4; see Table 3).

5. Discussion

5.1. Magnetostratigraphy

In order to resolve the North American (NA) APWP controversy blamed on IE of sedimentary rocks, the magnetization age should be well defined. For most units, the age is approximately bracketed by the unconformity ages (Anderson and Lucas, 1996; Lucas, 2018, 2004; Lucas and Anderson, 1998; Pipiringos and O'Sullivan, 1978), and for some, by biostratigraphic information provided in the literature (Imlay, 1980; Lucas, 2010; Wilcox and Currie, 2008). For example, the age of the Redonda Formation is late-Norian to Rhaetian, determined by correlation of the Apachean land-vertebrate faunachron (LVF) (Lucas and Hunt, 1993), which is pinned by the first appearance of a tetrapod genus "*Redondasaurus*" (ca. 215 Ma) (Fig. 11) to the standard global chronostratigraphic scale (Lucas, 2010). The magnetostratigraphy pattern of each unit was then used for correlation with the geomagnetic polarity time scales (GPTSs) an determining the magnetization age of corresponding units. The resulting magnetostratigraphy of the sampled units is proposed in Fig. 11.

For the Late Triassic, a chart proposed by Hounslow and Muttoni (2010), and for the Middle to Late Jurassic, a chart from Ogg et al. (2012), were considered as GPTS references for the units studied here. The Trujillo Formation is dominated by normal polarity zones and is correlated with UT13n, as the formation occupies Carnian-Norian boundary (Lucas, 1995) (Fig. 11). The Redonda Formation acquired most of its magnetization during reverse polarity chron, such as after ca. 215 Ma, so is correlated with UT18 (Fig. 11). Finally, the Lower-Oxfordian Summerville Formation is correlated with the Callovian-Oxfordian N and early-Oxfordian R zones (Fig. 11).

5.2. Implication for North American (NA) APWP

Two contradictory NA APWPs have been proposed for most of the Jurassic (e.g., Hagstrum, 1993). Results from well-dated kimberlite volcanics have been used to support a higher-latitude APWP (Kent et al., 2015; Kent and Irving, 2010). Disparity between APWPs was blamed on the inclination error (IE) in the paleomagnetic results of sedimentary units, most of which are from the U.S. South Western interior. Paleomagnetic poles from those define the other, lower-latitude path (Kent and Irving, 2010).

The two APWPs have the largest separation in the middle of the Jurassic, the age of the Summerville Formation. The zone-mean directions of the Summerville Formation are superimposed on the paleomagnetic direction trajectories predicted from the controversial APWPs for east-central New Mexico coordinates in Fig. 12. The zone-mean directions, specifically those from reversed zones, are in better agreement with the predicted trend calculated from Beck and Housen (2003) path than predicted by the high latitude path. This supports the lower-latitude APWP for North America, proposed by many studies (e.g., Beck and Housen, 2003; Gordon et al., 1984; May and Butler, 1986). Although some zone-mean's a95 confidence cone (e.g., MB-N1) encompasses both trends, it could be due to the small number of directions used to define the mean (n = 4, see Table 2) and/or an unremoved normal overprint. Moreover, the Summerville Formation reversed-zone means cluster around the 170 – 160 Ma sector of the predicted directional trend (Fig. 12), which is consistent with the suggested mean magnetization age (ca. 163 Ma) for this formation (Table 4). This also strengthens the conclusion that this ChRM component is most likely of primary origin as indicated by the fold and reversal tests results of the Summerville Formation (Fig. 8 and 9b).

Most of the sets (rock units) have been deposited in low sedimentation rate environments and

most of our zones encompasses several meters of sections (e.g., in zone TB-R, thickness=27m, and n=78, see Table 1 and 2). Therefore, PSV might have been averaged in the sample-level data such that zone VGPs would be good approximations of the paleopole for the corresponding zones. This would also imply that the A95s (95% confidence circles about the poles) should be used for poles in Fig. 13a. The VGPs of the zones (excluding excursions/transitions, and zone H01-TA-R) are shown in Fig. 13a (also see Table 2). Calculation of most zone-mean directions was by combining line and GC fits, so calculation of A95s for zone VGPs was not possible by simple transformation of the sample directions to pole coordinates. Instead, we used the precision parameters of the zone-mean directions and their paleolatitudes (calculated using the Dipole Formula: tan[magnetic inclination]=2 tan[latitude]) in Cox's (1970) method to determine corresponding A95s (Fig. 13a). All of the Late Triassic poles are perfectly streaked along the 245-200 track of the lower-latitude APWP, and the Middle Jurassic poles approximately hover around the 160 Ma cusp of the same path (Fig. 13a).

For the well-sampled formations, paleopoles were also calculated (Fig. 13b, and Table 4). Note that only reverse zone-mean directions were used for the Middle Jurassic formations to avoid possible bias from normal overprint. In order to find the mean directions for the formations (Dec and Inc in Table 4), the corresponding zone-mean directions were averaged using PMAG Tools v. 4.2a (Hounslow, 2006). This combines multiple paleomagnetic mean direction using their Fisher (1953) statistics and estimates the overall mean direction and precision parameters as if they had been calculated directly from all directions in the multiple zones. From those Formation mean, paleopoles were calculated from those mean directions (Table 4).

Although the E/I analysis for the IE were not robust, the flattening factors (*f*'s) estimated are in the range expected for hematite-bearing sediments (e.g., Kent and Tauxe, 2005) (except for

the Morrison Formation). Thus, we employed those *f*'s (Table 3) to correct the formation mean direction and consequently calculated corresponding IE-corrected paleopoles. These are for the Garita Creek and Trujillo Formations (ca. 223 Ma) at 55.7°N, 078.7°E, A95=3.2°, the Redonda Formation (ca. 214 Ma) at 59.7°N, 081.0°E, A95=4.0°, the Summerville Formation (ca. 163 Ma) at 59.3°N, 138.1°E, A95=6.5°, and the Lower Morrison Formation (Salt Wash Sandstone) (ca. 155 Ma) at 48.7°N, 151.8°E, A95=7.8° (see Table 4, and Fig. 13b).

As mentioned earlier, Steiner (2003) sampled and studied the cratonic Summerville Formation. Those samples were taken from the Romeroville Gap near Las Vegas, NM (this study's Las Vegas section) and the Trujillo Mound sections (locations L and T in Fig. 1). In the former locality, only first ~10 m mudstone-dominated section was interpreted and reported as the Summerville Formation (Steiner, 2003), and the rest of the section was assigned to the Lower and Upper Morrison Formation (Steiner et al., 1994). However, more recent paleontology and stratigraphy studies showed that the lower ~50 m part of the Las Vegas section, which is pale-red fine sandstone and mudstone, and which Steiner (2003) interpreted as the Lower Morrison is actually the Upper Summerville strata and is homotaxial with the Bluff Sandstone of San Rafael Group (Lucas, 2018; Lucas et al., 1999; Lucas and Woodward, 2001). Therefore, at Las Vegas locality the Salt Wash Sandstone of Morrison Formation, characterized by yellowish-brown coarse-grained, trough-crossbedded sandstone containing some clay clasts (Lucas et al., 1999) is as thin as ~5 m (Lucas, 2018). This means that the J-5 unconformity of Pipiringos and O'Sullivan (1978) at the base of the Salt Wash Sandstone occurs much farther up-section than previously thought, which was also confirmed by our field observations.

Correction for IE did not move the Summerville Formation paleopole toward the high-latitude APWP of Kent and Irving (2010) (Fig. 13b). Furthermore, we used three reported Summerville

Formation paleomagnetic poles to simulate the position of corresponding IE-corrected poles (Fig. 14). Two are from cratonic parts of NA (this study [52.4°N, 126.1°E], and Steiner (2003) [56.9°N, 143.3°E]) and one from the Colorado Plateau reported by Bazard and Butler (1992) corrected for 10.5° clockwise rotation of the plateau estimated by Beck and Housen (2003) [48.8°N, 142.7°E], . IE-corrected inclinations were calculated using King's (1955) equation and a range of *f* values (0.9-0.1), and then the new sets of declination and inclination were transformed to pole coordinates (Fig. 14). From Fig. 14 it is evident that no amount the IE correction of the sedimentary rocks from the SW portion of NA would bring two contradictory APWPs into an agreement. In other words, the sense of movement for the directions of the cluster of IE-uncorrected Summerville Formation poles must have been ~90° apart from what is currently estimated via IE-correction simulation, if the inclination shallowing was responsible for the NA APWP discrepancy (Fig. 14).

The high-latitude APWP proposed by Kent and Irving (2010) has few poles for Mid- to Late-Jurassic times. The 160 Ma mean pole, is based on four poles and only one of them is from NA, which is Moat volcanics (Van Fossen and Kent, 1990). The data come from a collapsed caldera, so paleohorizontal control may be suspect. More recently paleomagnetic results (sample VGPs) from radiometrically-dated Triple B (ca. 154.9 Ma) and Peddie (ca. 157.5 Ma) kimberlites established a ca. 156 Ma mean paleomagnetic pole (75.5°N, 189.5°E, A95=2.8°, K=79, n=34) (Kent et al., 2015), which was used to support the high-latitude APWP. Besides the lack of paleohorizontal control in these kimberlites, the lower A95 limit for combined Triple B and Peddie pole is 2.9° (calculated via method of Deenen et al., 2011), which shows that PSV may not have been adequately sampled. Therefore, the high-latitude APWP suffers from inadequately-sampled PSV and lack of vigorous paleohorizontal control, although we think that the latter should be the prime suspect. Poles for other ages along the high latitude path derived

from northeastern NA might also suffer from regional tilt due to vertical movement of the continental margin as a consequence of post-rifting thermal uplift/subsidence.

Data and analysis presented here indicate that even with IE-correction the NA APWP would streak approximately along 60° parallel (in current coordinates) for most of the Jurassic, and the lingering APWP discord is not rooted in IE of the sedimentary units.

6. Conclusions

Paleomagnetic results of Upper Triassic (Garita Creek, Trujillo, and Redonda Formations), and Middle Jurassic (Entrada, Summerville, and Lower Morrison Formations) sedimentary units of east-central New Mexico has revealed magnetostratigraphy that is correlated with the GPTS's, although more detail work is required to achieve better-constrained magnetization ages. Most of the sampled units are fine-grain sandstones, siltstones, and mudstones that rock-magnetic analysis indicated hematite (mostly detrital) as the main remanence carrier.

In a general sense, paleomagnetic data for the Upper Triassic units has better quality than for the Middle Jurassic ones, which, nevertheless pass fold and reversal tests. The lesser quality of the Middle Jurassic data could be due to high rate of polarity reversals for this time period (Biggin et al., 2008). Abundance of great-circle fits to demagnetization data greatly reduced the number of sample-level directions that could be used to evaluate inclination error (IE) using the elongation/inclination (E/I) method of Tauxe and Kent (2004). Despite large flattening factors (*f*'s), IE is negligible for Upper Triassic units because the mean direction is horizontal ($I_O = 0.4$; see Table 3). The E/I results estimate ~20° IE for the Middle Jurassic units, however, their 95% confidence limits are too large (~25°), attributable to the small number of directions (n=62) used and existence of an additional source of scatter in the distribution of directions besides paleosecular variation (PSV). This additional source of scatter is confirmed by using A95 criteria of Deenen et al. (2011), and it is likely due to polar wander and probably denotes that the time span of the corresponding paleomagnetic directions used for the E/I analysis is large relative to the high rate of the polar wander.

Most of the units were deposited in low sedimentation-rate environments and most of our zones encompasses several meters of sections, so the PSV might have been already averaged

within zones, thus a zone VGP might be a good approximation of the paleopole for the corresponding zone. Additionally, we combined paleomagnetic directions from zones within units to define formation-mean directions and paleopoles for Trujillo, Redonda, Summerville, and Lower Morrison (Table 4). Data and analysis presented here indicate that even with IE-corrected directions, poles for the North American (NA) APWP would streak approximately along 60° parallel for most of the Jurassic times, which validates the lower-latitude APWP for NA.

Simulation of Middle Jurassic poles from existing ones assuming possible range of *f*'s show (Fig. 14) that no amount of the IE correction to the results from these sedimentary units would produce poles consistent with the high-latitude APWP of Kent and Irving (2010). If the discrepancy between the two APWPs is not due to IE of the sedimentary units from southwest NA, could it be due to some errors in results from the Northeast? We suggest that ca. 156 Ma paleopole determined by kimberlite-type volcanics (Kent et al., 2015), which is the main support of high-latitude APWP, suffers from inadequately-sampled PSV. This along with general lack of vigorous paleohorizontal control in input-poles of high-latitude APWP could be the prime suspects of NA APWP discord.

7. Tables

Table 1: Set and zone divisions at each sampled locality. Zones are 'N' and 'R' for normal and reverse polarity zones, respectively. * Transition (T) and excursion (E) zones are distinguished where ever a group of stratigraphically consecutive samples has shown characteristic remanence directions (and their mean) with more than 40° deviation from the mean direction of the surrounding polarity zones. 'Transitions' represent the completion of the reversal whereas 'excursions' are only deviations from dipole geomagnetic field, long enough to be preserved. ** is discarded from further analysis, due to initially undetected local crumpling in the sampled horizon. lat. and long.: coordinates of the sampling sites, sst: sandstone, sltst: siltstone, mdst: mudstone, ls: limestone, sh: shale, x-bd: cross-bedding, t.d.: thin-bedded, alt: altered, nod: nodule, Fm: Formation, Mbr: member.

Set	Zone	Coordinates		Lithostratigraphic unit	Bedding attitude		Lithology	Apprx. thickness (m)	Apprx. sampling spacing (m)
		Lat.	Long.		Dip direction (°)	Dip (°)			
Trujillo Mound									
TD	TD-R1	35.519	255.307	Morrison Fm. / Salt Wash Sst	Horizontal		creamy sst	10	1
TC	TC-N1	35.516	255.310	Entrada Fm. / Slick Rock Mbr.	060	06	tan sst, with x-bd (eolianite)	7	1.5
	TC-T1*	35.516	255.310	Entrada Fm. / Slick Rock Mbr.	060	06		1.5	1.5
TB	TB-R	35.514	255.316	Redonda Fm.	327	03	red sst. & mdst.	27	0.4 - 0.5
TA	H02 (TA-N)	35.514	255.316	Redonda Fm.	Horizontal		white ls.	1	0.4 - 0.5
	H01 (TA-R)	35.514	255.316	Redonda Fm.	**			1	0.4 - 0.5
Mills Canyon									
MC	MC-R1	35.912	255.650	Morrison Fm.	310	04	pale gray sst.	1-2	1
	MC-N1	35.912	255.650	Morrison Fm.	310	04		3-4	1
MB	MB-R1	35.913	255.653	Summerville Fm.	324	04	red sltst. & mdst. / with alabaster nod.	8	0.4
	MB-N1	35.913	255.653	Summerville Fm.	302	05		0.5	0.4
MA	MA-E2*	35.914	255.652	Entrada Fm. / Exeter Mbr.	280	04	mud-support sst.	1	1
	MA-E1*	35.914	255.652	Entrada Fm. / Exeter Mbr.	280	04		5	1
Las Vegas									
LA	LA-R2	35.525	254.759	Morrison Fm. / Salt Wash Sst.	074	30	creamy sst.	6	1-2
	LA-N2	35.525	254.759	Summerville Fm.	067	32	pale red sst. & sltst. with sh. & mdst.	15	1-2
	LA-T2*	35.525	254.759	Summerville Fm.	074	30		3	1-2
	LA-R1	35.525	254.759	Summerville Fm.	073	26		20	1-2
	LA-T1*	35.525	254.759	Summerville Fm.	074	30		2	1-2
	LA-N1	35.525	254.759	Summerville Fm.	078	32		6	1-2
	H01 (LA)	35.525	254.759	Todilto Fm.	074	30	dark gray ls.	1-2	0.4 - 0.5
Romeroville exit									
RC	RC-N	35.517	254.755	Trujillo Fm.	065	12	creamy sst.	8	0.5 - 1
RB	RB-N	35.517	254.755	Trujillo Fm.	073	15	t.b. sst.	20	0.3
RA	RA-N	35.517	254.755	Garita Creek Fm.	076	12	red sst. & sltst.	3	0.1 - 0.15
Conchas Lake									
CB	CB-E1*	35.298	255.708	Trujillo Fm.	268	02	creamy sst. with large x-bd	6	1
	CB-N1	35.298	255.708	Trujillo Fm.	268	02		8	1
CA	CA-N1	35.298	255.708	Trujillo Fm.	355	08	red sltst.	1.5	0.2

Table 2: Paleomagnetic directions of Upper Triassic and Middle Jurassic strata from east-central New Mexico. n/N: number of directions used to calculate the zone mean/ total number of specimens; Dec and Inc: tilt-corrected declination and inclination of the characteristic remanent magnetization (ChRM) component; a95 and k: half-angle of the 95% confidence limit and precision parameter of Fisher (1953) statistics; R: length of the resultant vector; L/GC: number of line fits (principal component analysis of Kirschvink [1980]) / great-circle fits to calculate the mean (McFadden and McElhinny, 1988); Lat. (Long.): north latitude (east longitude) of the paleopole (negative sign indicates south latitude).

Set	Zone	n/N	L /GC	Raw data							Smoothed data						
				Mean direction					VGP		Mean direction					VGP	
				Dec	Inc	a95	k	R	Lat.	Long.	Dec	Inc	a95	k	R	Lat.	Long.
Trujillo Mound																	
TD	TD-R1	21/41	1/20	129.4	-36.9	11.5	8.63	18.74	-43.5	340.7	128.4	-37.5	11.1	9.18	18.88	-42.8	341.8
TC	TC-N1	9/13	9/-	348.4	49.1	17.0	10.17	8.21	78.8	139.0	350.0	43.0	15.9	11.50	8.30	76.4	117.4
	TC-E1	5/5	5/-	053.1	56.2	28.6	8.09	4.51	47.6	327.3	053.4	53.1	29.5	7.67	4.48	46.6	331.7
				TB unit mean direction without excluding excursion zones													
TB	TB-R	78/112	45/33	176.6	-04.3	7.2	5.79	67.56	-56.5	261.5	177.2	-04.2	6.6	6.71	68.98	-56.5	260.5
				TB unit mean directions, excluding excursion zones													
TB	TB-E5	3/3	2/1	135.5	-55.5	15.3	179.22	2.99	-54.2	359.5	148.2	-56.0	32.7	40.18	2.98	-64.3	357.0
	TB-R5	16/20	7/9	161.1	-07.8	10.5	13.50	15.15	-53.9	288.6	167.4	-09.8	10.1	13.59	16.12	-57.3	279.0
	TB-E4	15/21	6/9	218.9	48.7	27.6	2.75	11.00	-15.2	220.9	201.1	57.8	27.5	2.63	11.44	-13.5	238.5
	TB-R4	14/20	4/10	185.3	-02.8	16.4	6.86	12.40	-55.5	246.0	178.4	-05.5	16.8	5.75	13.74	-57.2	258.2
	TB-E3	1/3	1/-	241.8	22.8	-	-	1.00	-14.9	192.1	240.9	26.1	-	-	1.00	-14.3	194.2
	TB-R3	5/6	4/1	157.2	11.9	5.1	354.93	4.99	-43.2	287.3	160.5	11.6	5.4	318.79	4.99	-44.7	283.2
	TB-E2	4/9	4/-	218.1	-01.9	9.5	94.18	3.97	-40.5	201.0	212.9	00.0	10.2	82.78	3.96	-43.1	207.2
	TB-R2	5/6	3/2	178.0	-17.7	28.2	10.25	4.76	-63.5	259.6	185.4	05.1	27.2	9.90	4.70	-51.6	246.6
	TB-E1	2/3	1/1	220.4	09.1	-	14.27	1.97	-34.9	203.4	230.1	03.8	13.0	3878.78	2.00	-30.1	192.8
	TB-R1	12/21	4/8	169.1	15.7	8.9	25.15	11.64	-45.3	270.8	174.1	07.6	10.0	18.83	12.52	-50.3	264.6
TA	H02 (TA-N)	3/9	1/2	355.0	14.3	14.5	100.368	2.99	61.4	85.8	355.4	14.1	13.7	112.95	2.99	61.3	084.8
	H01 (TA-R)	5/5	5/-	155.5	-36.2	16.5	22.36	4.82	-63.6	316.2	152.8	-33.4	9.1	71.21	4.94	-60.4	316.8
Mills Canyon																	
MC	MC-R1	4/9	2/2	132.1	02.8	57.7	4.2	3.53	-31.9	316.6	159.8	1.5	22.7	22.9	3.91	-48.8	287.2
	MC-N1	5/7	5/-	314.8	41.6	28.5	8.2	4.51	49.4	161.3	314.9	41.9	27.8	8.5	4.53	49.6	161.6
MB	MB-R1	24/26	17/7	153.6	-18.2	10.7	8.6	22.31	-54.2	304.2	151.3	-16.3	11.0	8.1	22.21	-52.0	306.2
	MB-N1	4/5	1/3	343.1	32.0	25.5	15.5	3.84	66.1	119.1	343.6	29.8	20.8	22.9	3.89	65.3	116.1
MA	MA-E2	3/5	2/1	212.8	17.2	-	3.2	2.68	-35.7	214.4	250.3	22.0	91.1	6.5	2.85	-8.7	186.6
	MA-E1	12/13	8/4	100.8	-13.5	28.4	3.2	9.19	-12.7	344.9	103.5	-10.9	32.3	2.7	8.63	-14.2	342.2
Las Vegas																	
LA	LA-R2	5/6	1/4	146.6	-44.6	24.4	16.0	4.87	-60.1	336.1	150.9	-36.6	21.2	20.9	4.90	-60.3	321.8
	LA-N2	7/22	6/1	313.5	42.4	19.1	11.2	6.51	48.7	162.5	310.7	37.9	19.1	11.2	6.51	44.8	160.1
	LA-T2	4/6	1/3	82.3	-33.9	47.3	7.8	3.81	-04.7	004.3	091.0	-42.7	30.2	18.0	3.92	-14.9	004.8
	LA-R1	21/28	10/11	152.8	-15.8	15.3	5.1	18.19	-53.0	303.5	151.5	-17.5	13.5	6.5	18.75	-52.8	303.1
	LA-T1	6/6	6/-	283.9	73.3	46.2	3.1	4.37	36.8	216.1	294.0	72.4	48.3	2.9	4.26	41.9	213.6
	LA-N1	8/10	8/-	330.5	39.3	19.7	8.9	7.21	61.1	145.4	331.3	36.4	20.0	8.7	7.19	60.5	141.3
	H01 (LA)	2/3	1/1	159.2	-18.4	-	7.5	1.93	-57.8	295.8	154.7	-18.8	-	5.5	1.91	-55.3	302.6
Romeroville exit																	
RC	RC-N	21/58	21/-	001.9	05.8	13.1	6.8	18.08	57.3	071.2	001.3	03.6	13.0	7.0	18.12	56.3	072.4
RB	RB-N	9/26	9/-	350.4	05.7	20.9	7.0	7.86	56.2	092.1	351.7	8.1	20.3	7.4	7.92	57.6	090.4
RA	RA-N	23/64	22/1	003.7	-04.5	8.2	14.7	21.54	52.1	068.7	004.7	-3.5	6.1	25.2	22.15	52.5	067.1
Conchas Lake																	
CB	CB-E1	4/17	1/3	050.0	-53.4	33.7	14.6	3.90	06.5	035.9	049.5	-56.7	36.3	12.7	3.88	04.1	038.4
	CB-N1	13/35	1/12	350.2	-00.3	13.6	10.2	11.88	53.4	092.4	348.7	-00.4	15.1	8.5	11.65	53.0	094.7
CA	CA-N1	9/18	9/-	351.7	03.3	7.0	55.3	8.86	55.4	090.5	351.8	03.1	6.8	59.1	8.86	55.4	090.3

Table 3: Results of E/I analysis (Tauxe and Kent, 2004) of sample-level directions from line fits of Upper Triassic and Middle Jurassic formations of east-central New Mexico. A95 (95% confidence circle about the paleomagnetic pole) of all Jurassic formations are slightly higher than Deenen et al. (2011) criteria, which indicates that the dispersion of VGPs has sources other than paleosecular variation (PSV) (see text for further explanation). *: Sample-level Summerville Formation directions of Steiner (2003) from her Trujillo section; N: number of directions in each dataset; D and I_O: declination and inclination of the observed mean direction; f: flattening factor determined from E/I analysis; I_C: corrected mean inclination; +/- I_C: 95% confidence limits for I_C calculated from 1000 bootstraps; Plat, Plong, and A95 (Plat´, Plong´, and A95´): coordinate of the paleopole and radius of its 95% confidence circle calculated from the distribution of VGPs (IE-corrected directions transformed to VGPs); A95min and A95max: upper and lower limits of A95, which provide reliability criteria to examine the role of PSV in dispersion of the paleomagnetic VGPs (Deenen et al., 2011).

Formation	N	D (°)	I_O (°)	*f*	I_C (°)	+/- I_C (°)	Plat´	Plong´	A95´	Plat	Plong	A95	*Deenen et al. (2011) criteria*		
													A95max	*A95min*	*A95 criteria*
upper Triassic units	120	359.1	00.40	0.43	00.46	0.1 - 9.3	55.6	076.7	4.9	55.3	076.9	4.0	*4.0*	*1.8*	*ok*
Summerville Fm.	34	329.1	28.45	0.44	49.06	33.3 - 62.5	63.7	163.6	9.8	56.6	137.6	9.4	*8.9*	*2.9*	*too high*
Morrison Fm.	28	314.0	36.20	0.98	36.72	32.8 - 66.7	47.4	160.6	10.9	47.2	160.1	10.9	*10.0*	*3.2*	*too high*
Summerville Fm. & Morrison Fm.	62	322.6	31.80	0.49	50.65	37.4 - 61.6	59.1	170.6	7.3	52.9	148.9	7.3	*6.1*	*2.3*	*too high*
Summerville Fm. & Summerville Fm. *	96	324.5	35.96	0.46	57.61	44.2 - 69.2	61.8	183.3	6.3	56.1	152.3	6.6	*4.6*	*1.9*	*too high*

Table 4: Paleomagnetic pole coordinates of Upper Triassic and Middle Jurassic units of east-central New Mexico for the well-sampled formations of this study. Age is the mean age inferred from both Fig. 14 and the literature (Pipiringos and O'Sullivan (1978) for the Salt Wash Member); N: sum of the sample directions from all averaged zones; Dec and Inc: declination and inclination of the mean direction; f: flattening factor determined from E/I analysis (see Table 3); Inc': corrected mean inclination; Plat, Plong, and A95 (Plat´, Plong´, and A95´): coordinates of the paleomagnetic pole and its radius of 95% confidence circle indirectly calculated using Cox's (1970)(same but from IE-corrected means).

Formation	Age (Ma)	Mean unit coordinates		Mean direction				*f*	Inc'	Pole coordinates					
		Lat.	Long.	N	Dec	Inc	a95			Plat.	Plong.	A95	Plat'	Plong'	A95'
Middle Jurassic															
Morrison (Salt Wash Mbr)	155	35.573	255.261	30	137.5	-32.8	10.1	0.98	-33.3	48.5	151.4	7.7	48.7	151.8	7.8
Summerville	163	35.733	255.234	45	151.4	-16.9	8.4	0.46	-33.4	52.4	126.1	5.4	59.3	138.1	6.5
Upper Triassic															
Redonda	214	35.514	255.316	81	177.1	-4.6	6.5	0.43	-10.6	56.7	080.6	3.9	59.7	081.0	4.0
Garita Creek and Trujillo	223	35.453	255.035	75	357.9	01.1	5.2	0.43	02.6	55.0	078.7	3.2	55.7	078.7	3.2

8. Figures

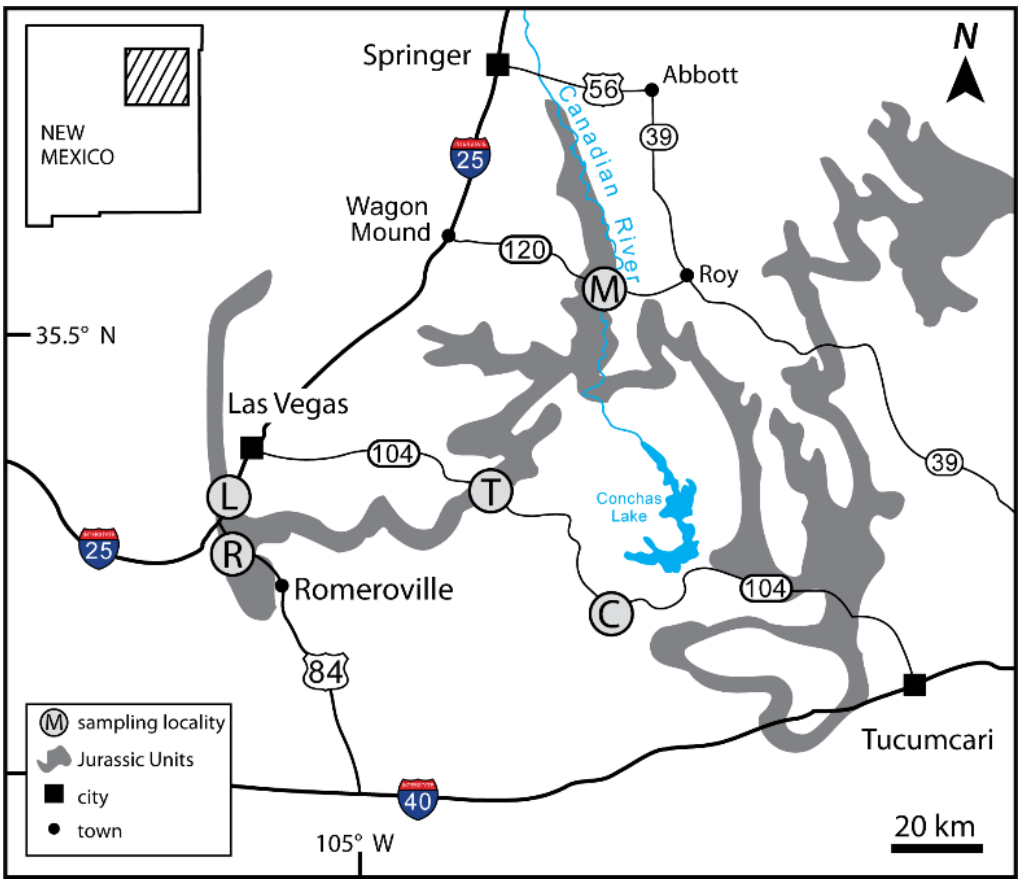

Fig. 1: Sampling localities in east-central New Mexico; R: Romeroville Exit, L: Las Vegas city, T: Trujillo Mound, C: Conchas Lake, M: Mills Canyon; The gray- shading shows the distribution of Middle to Upper Jurassic strata in the area [modified from Anderson and Lucas (1992)].

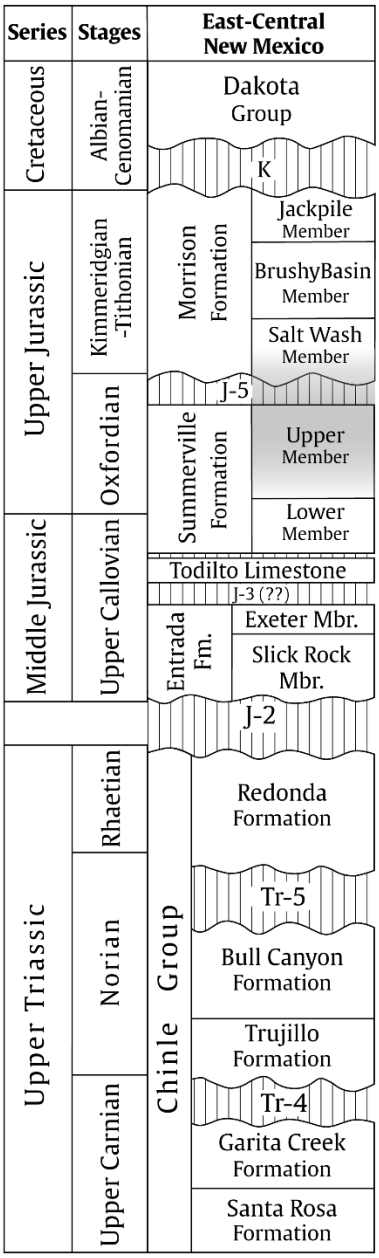

Fig. 2: Stratigraphy of Upper Triassic to Cretaceous strata in east-central New Mexico. Upper Triassic Stratigraphic column is modified from Lucas (2004, 1995), Jurassic is modified after Lucas (2018), Lucas and Woodward (2001), and Anderson & Lucas (1992), and Cretaceous is after Lucas et al. (1998). The shaded area was interpreted as Lower Morrison Formation in Las Vegas section (see Fig. 1) by Steiner et al. (1994).

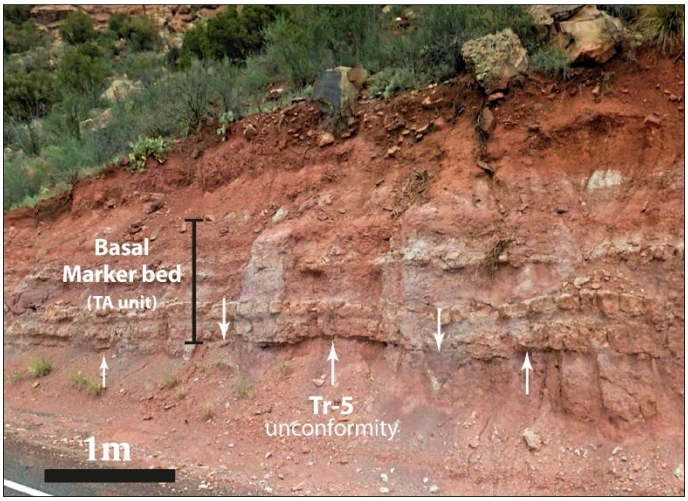

◄ **Fig. 3:** TA limestone unit, which is the Basal Marker bed (Hester and Lucas, 2001) of Redonda Formation of Upper Chinle Group. Arrows point to the Tr-5 unconformity.

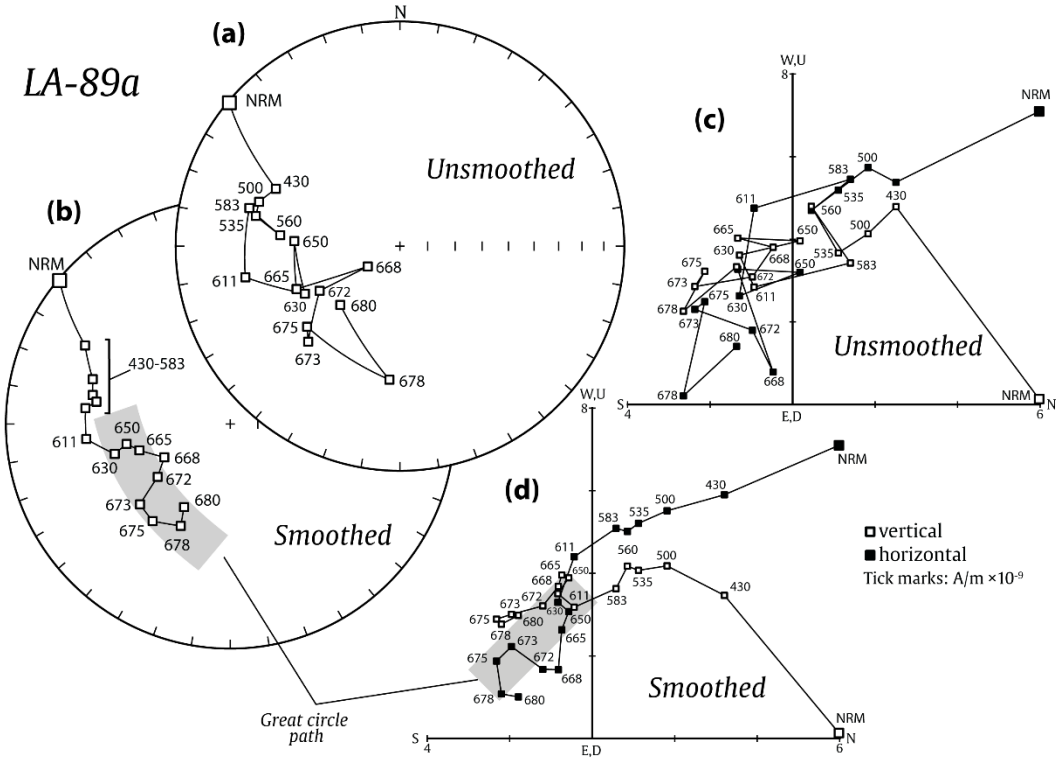

Fig. 4: Equal-area and orthogonal vector endpoint diagrams (before tilt correction) of raw (a, and c) and smoothed (b, and d) data for a representative thermally demagnetized sample from LA-R2 zone. The contrast shows the effectiveness of the averaging scheme to decrease noise in the data. Note that the great-circle path of remanence vectors (650 – 680 °C) was not perceivable before smoothing.

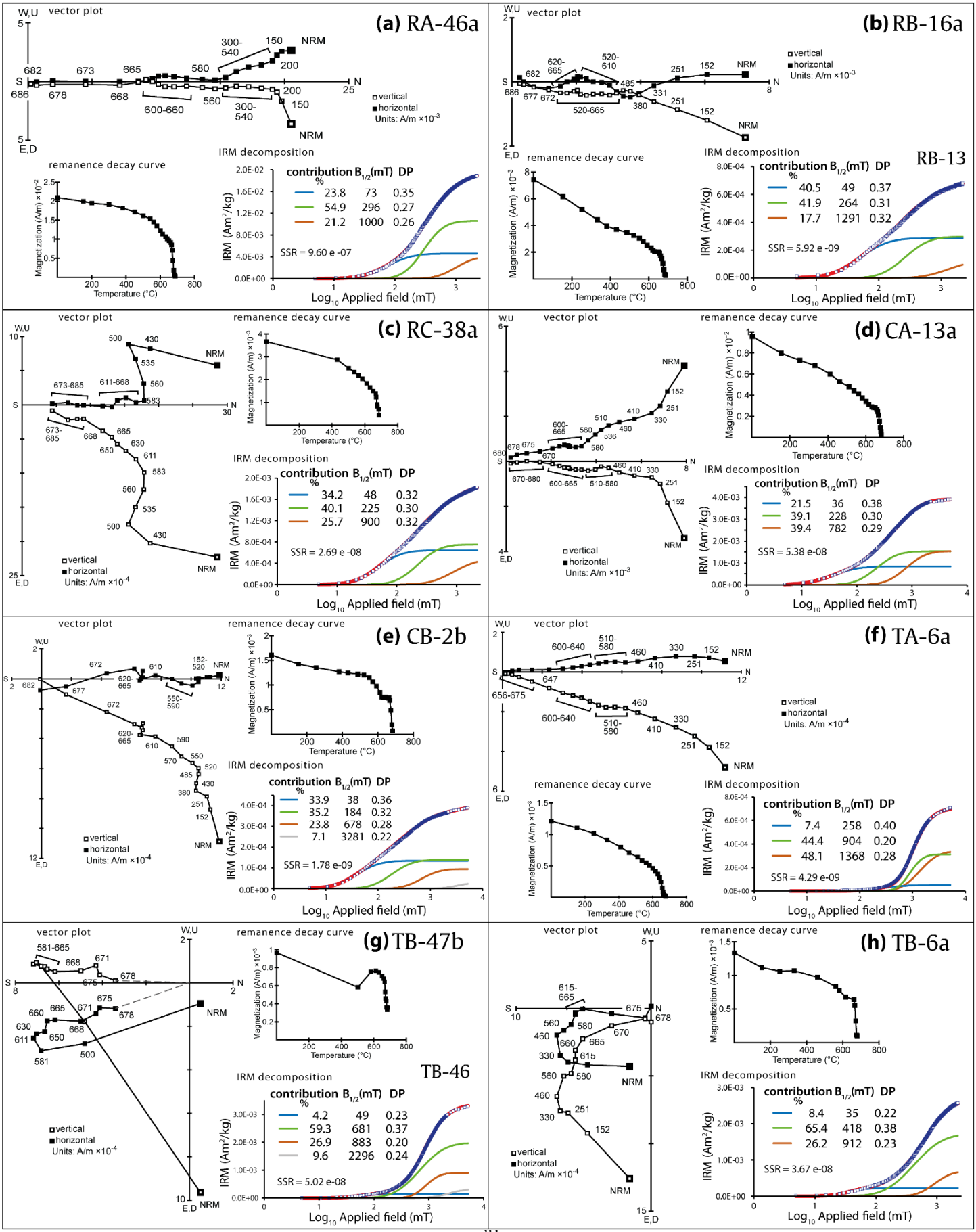
(a) RA-46a
vector plot
W,U
E,D
S
N
NRM
vertical
horizontal
Units: A/m ×10-3
remanence decay curve
Magnetization (A/m) ×10-2
Temperature (°C)
IRM decomposition
contribution B1/2(mT) DP
%
23.8 73 0.35
54.9 296 0.27
21.2 1000 0.26
SSR = 9.60 e -07
IRM (Am2/kg)
Log10 Applied field (mT)
(b) RB-16a
RB-13
Units: A/m ×10-3
contribution B1/2(mT) DP
%
40.5 49 0.37
41.9 264 0.31
17.7 1291 0.32
SSR = 5.92 e -09
(c) RC-38a
Units: A/m ×10-4
contribution B1/2(mT) DP
%
34.2 48 0.32
40.1 225 0.30
25.7 900 0.32
SSR = 2.69 e -08
(d) CA-13a
Units: A/m ×10-3
contribution B1/2(mT) DP
%
21.5 36 0.38
39.1 228 0.30
39.4 782 0.29
SSR = 5.38 e-08
(e) CB-2b
Units: A/m ×10-4
contribution B1/2(mT) DP
%
33.9 38 0.36
35.2 184 0.32
23.8 678 0.28
7.1 3281 0.22
SSR = 1.78 e-09
(f) TA-6a
Units: A/m ×10-4
contribution B1/2(mT) DP
%
7.4 258 0.40
44.4 904 0.20
48.1 1368 0.28
SSR = 4.29 e-09
(g) TB-47b
TB-46
Units: A/m ×10-4
contribution B1/2(mT) DP
%
4.2 49 0.23
59.3 681 0.37
26.9 883 0.20
9.6 2296 0.24
SSR = 5.02 e-08
(h) TB-6a
Units: A/m ×10-4
contribution B1/2(mT) DP
%
8.4 35 0.22
65.4 418 0.38
26.2 912 0.23
SSR = 3.67 e-08

▲ **Fig. 5:** Orthogonal vector endpoint diagrams and remanence decay curves of thermally demagnetized representative samples from Upper Triassic zones, with their isothermal remanent magnetization (IRM) plots (log-acquisition plot). (a-b, d-e) for zones of the Trujillo Formation (CA-N1, CB-N1, RB-N, and RC-N respectively). (c) for the RA-N zone of the Garita Creek Formation. (f) for the TA-N zone and (g-h) for the TB-R zone of the Redonda Formation. IRM decomposition results based on cumulative log-Gaussian (GLC) function (Kruiver et al., 2001). $B_{1/2}$ and DP are the mean coercivity and dispersion parameter of the GLC function. SSR is the sum of the squared residuals for IRM component fitting.

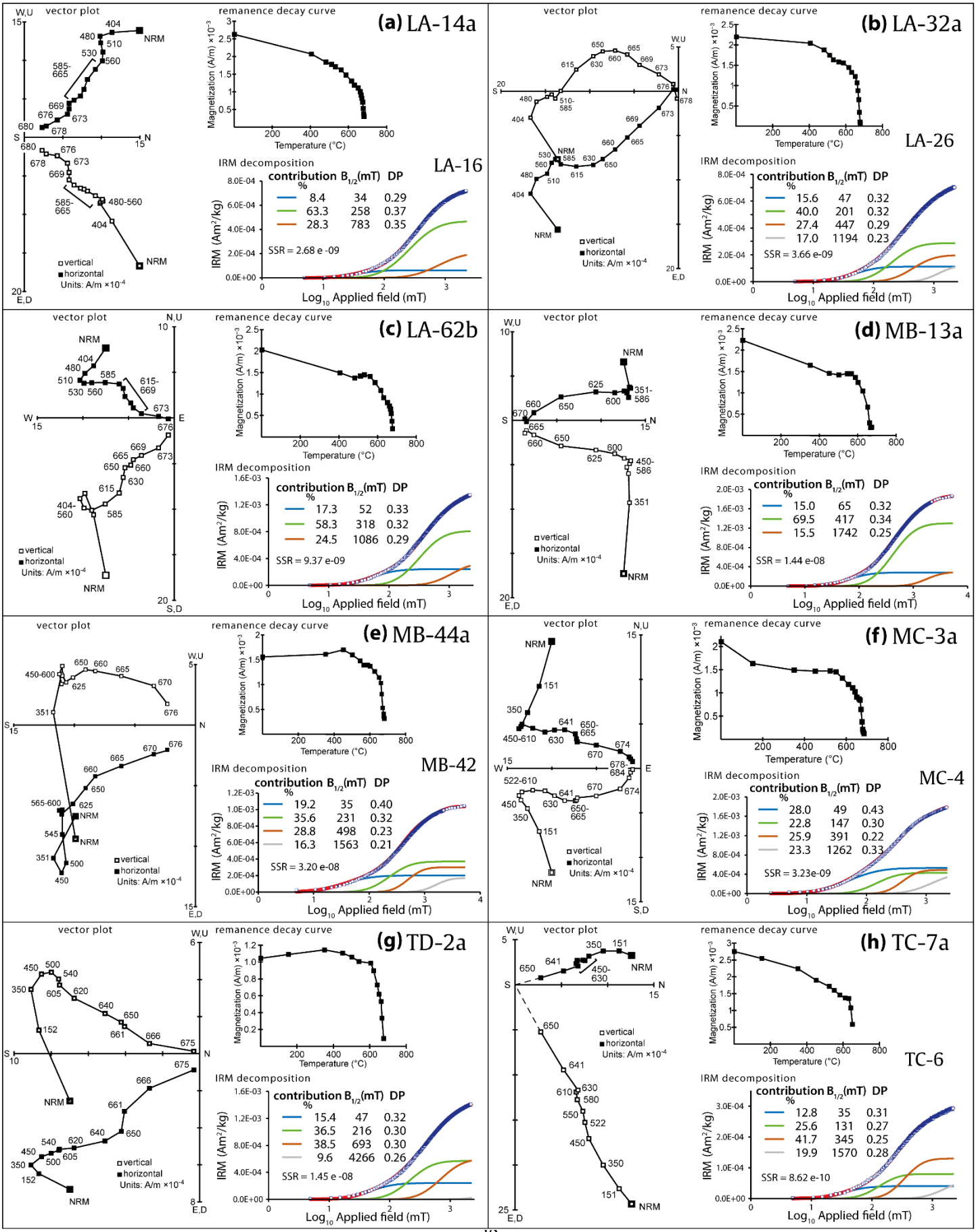
(a) LA-14a
vector plot
remanence decay curve
W,U
N
S
E,D
vertical
horizontal
Units: A/m ×10⁻⁴
Magnetization (A/m) ×10⁻³
Temperature (°C)
IRM decomposition
contribution B1/2(mT) DP
%
8.4 34 0.29
63.3 258 0.37
28.3 783 0.35
SSR = 2.68 e -09
IRM (Am²/kg)
Log10 Applied field (mT)
(b) LA-32a
LA-26
contribution B1/2(mT) DP
15.6 47 0.32
40.0 201 0.32
27.4 447 0.29
17.0 1194 0.23
SSR = 3.66 e-09
(c) LA-62b
LA-16
N,U
W
E
S,D
contribution B1/2(mT) DP
17.3 52 0.33
58.3 318 0.32
24.5 1086 0.29
SSR = 9.37 e-09
(d) MB-13a
contribution B1/2(mT) DP
15.0 65 0.32
69.5 417 0.34
15.5 1742 0.25
SSR = 1.44 e-08
(e) MB-44a
MB-42
contribution B1/2(mT) DP
19.2 35 0.40
35.6 231 0.32
28.8 498 0.23
16.3 1563 0.21
SSR = 3.20 e-08
(f) MC-3a
MC-4
contribution B1/2(mT) DP
28.0 49 0.43
22.8 147 0.30
25.9 391 0.22
23.3 1262 0.33
SSR = 3.23e-09
(g) TD-2a
contribution B1/2(mT) DP
15.4 47 0.32
36.5 216 0.30
38.5 693 0.30
9.6 4266 0.26
SSR = 1.45 e -08
(h) TC-7a
TC-6
contribution B1/2(mT) DP
12.8 35 0.31
25.6 131 0.27
41.7 345 0.25
19.9 1570 0.28
SSR = 8.62 e-10

▲ **Fig. 6:** Orthogonal vector endpoint diagrams and remanence decay curves of thermally demagnetized representative samples from Middle Jurassic zones, with their IRM plots (log-acquisition plot). (a-e) for zones of the Summerville Formation (LA-N1, LA-R1, LA-N2, MB-N1, and MB-R1 respectively). (f, h) for the MC-N1 and TD-R1 zones of the Morrison Formation. (g) for the TC-N1 zone of the Entrada Formation. See Fig. 5 for more information.

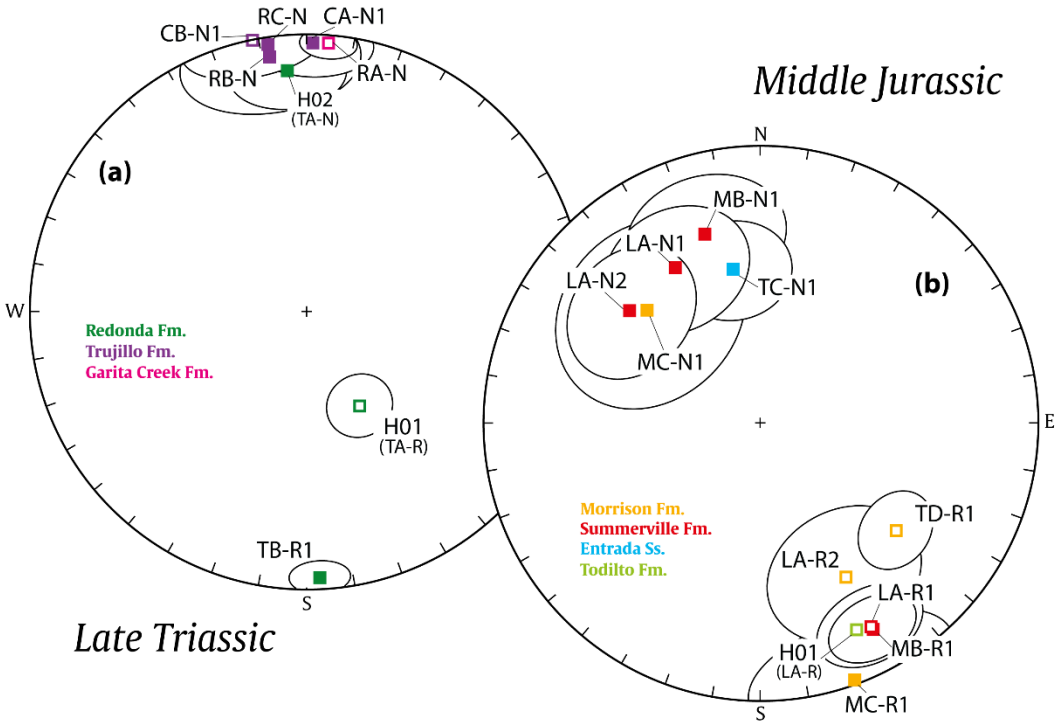

Fig. 7: Equal-area plots of zone-mean directions of (a) Upper Triassic and (b) Middle Jurassic units. Ellipses are the projection of the cone of 95% confidence limits about the mean directions (not drawn if >30°). TA-R mean direction is discarded from further analysis due to initially undetected local slumping in the sampled horizon.

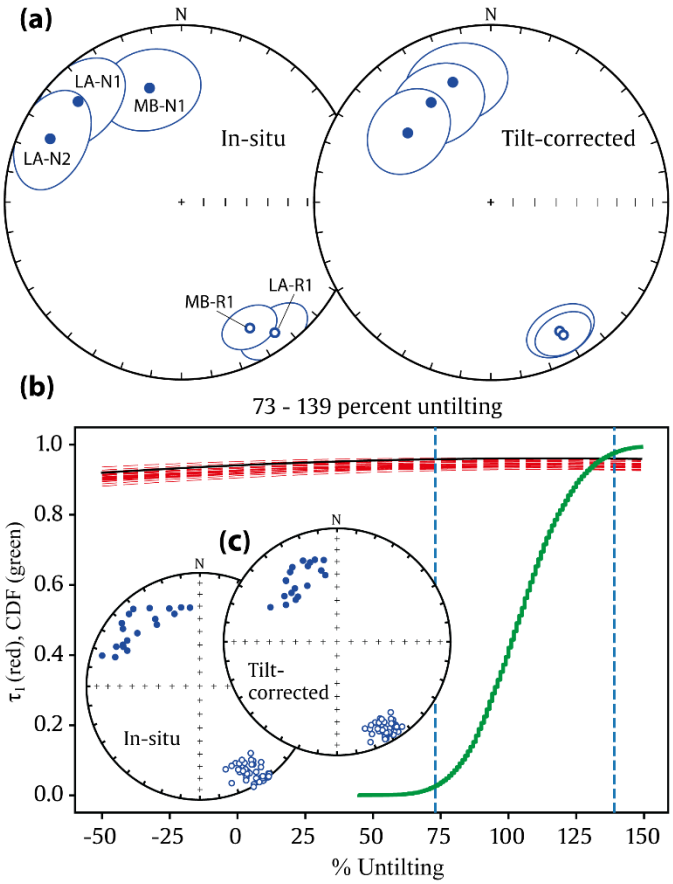

Fig. 8: Fold test results of Summerville Formation zones. (a) Equal-area plots of in-situ and tilt-corrected zone-mean directions. Ellipses are the projection of the cone of 95% confidence limits about the means. (b) positive bootstrap fold test (Tauxe and Watson, 1994) of simulated mean directions (see text for more explanation). The synthetic mean directions are adjusted for incremental tilting from -50% to 150%. (c) Equal-area plots of in-situ and tilt-corrected synthetic zone-mean directions. The test indicates the pre-tilting magnetization as the 95% confidence interval (vertical lines) of the largest eigenvalue (τ_1) encompasses 100% of untilting (73-139%). The number of bootstraps is 10k.

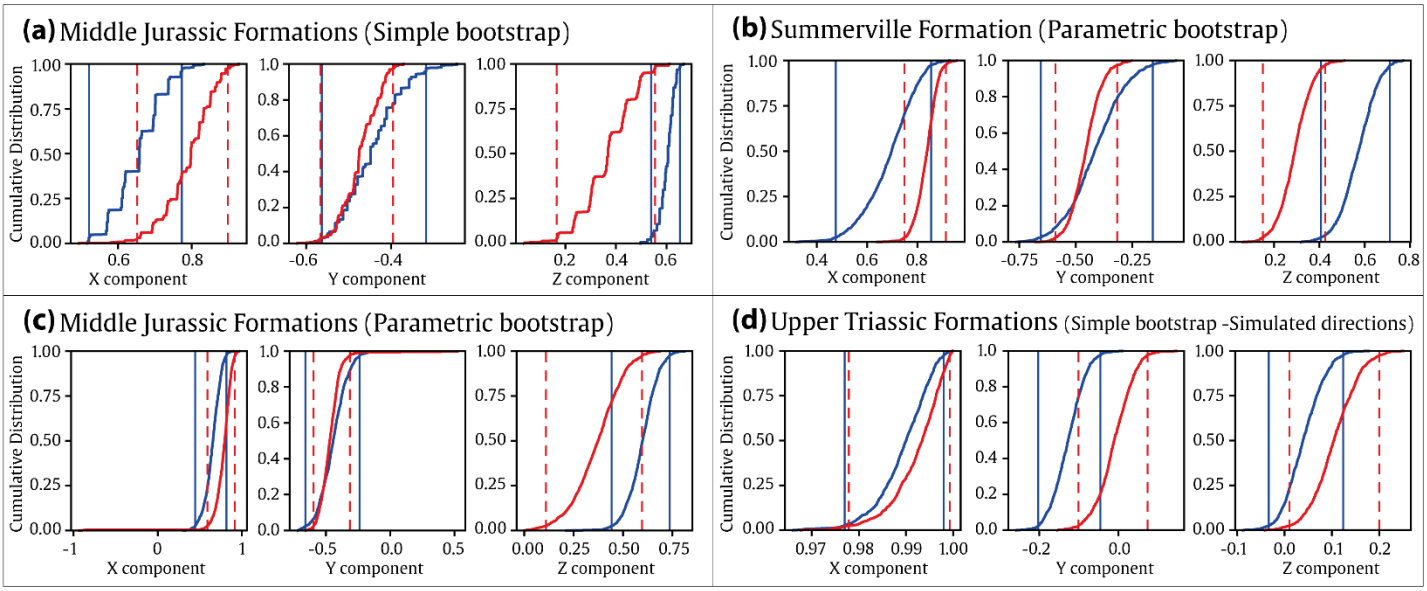

Fig. 9: Bootstrapped reversal test results for (a-c) Middle Jurassic and (d) Upper Triassic strata of east-central New Mexico. (a, and c) are simple (Tauxe et al. 1991) and parametric bootstrap test results for all nine zone-mean directions of Middle Jurassic Formations; (b) is the parametric bootstrap test on Summerville Formation zone means, and (d) is the result of simple bootstrap test (Tauxe et al. 1991) for Upper Triassic mean directions (because there is only one normal zone-mean direction, we simulated sample-level directions based on the statistical precision parameters (k,n) of zone mean directions and simple bootstrap reversal test was used). See text for more explanation. The graphics show the cumulative distribution of directions in Cartesian coordinates, with their 95% confidence intervals (vertical lines). The test is considered to be positive, if the 95% confidence intervals of all X, Y, and Z overlap (Tauxe et al., 1991).

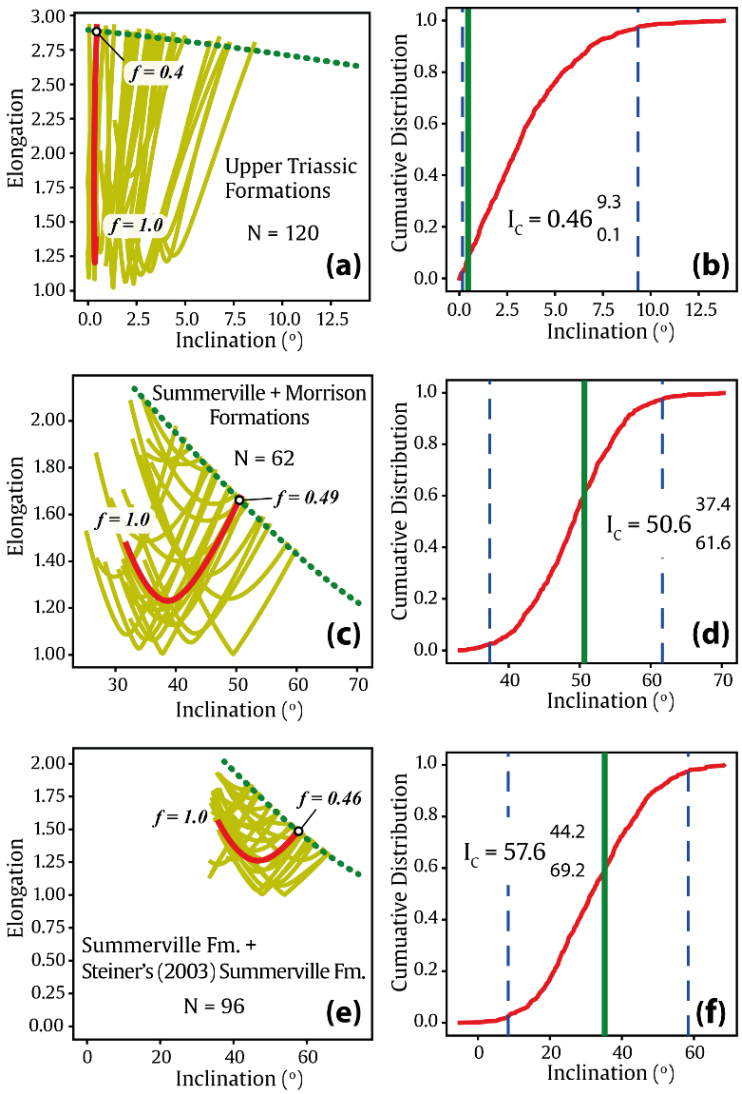

Fig. 10: Elongation/Inclination (E/I) analyses (Tauxe and Kent, 2004) on the sample-level line fits of (a-b) Upper Triassic and (c-d) Middle Jurassic (Summerville and Morrison) Formations of east-central New Mexico. (d-e) This study's Summerville Formation sample-level directions combined with Summerville Formation directions of Steiner (2003) from her Trujillo section. Graphs on the left side show trajectories of mean inclination versus elongation of bootstrapped distributions calculated with values of flattening factors (f) ranging from 0.3 to 1.0. The dotted line is the predicted E/I trend of the TK03.GAD geomagnetic field model; in each, the circle is labeled with f that corresponds to the bootstrapped E/I mean consistent with the field model. Right-side graphs are cumulative distributions of f's correspond to the 1000 E/I intersections in the left graphs with the dashed vertical lines showing the 95% confidence intervals. N: number of directions in each dataset; I_C: corrected mean inclination; +/- I_C: 95% confidence limits for I_C calculated from 1000 bootstraps.

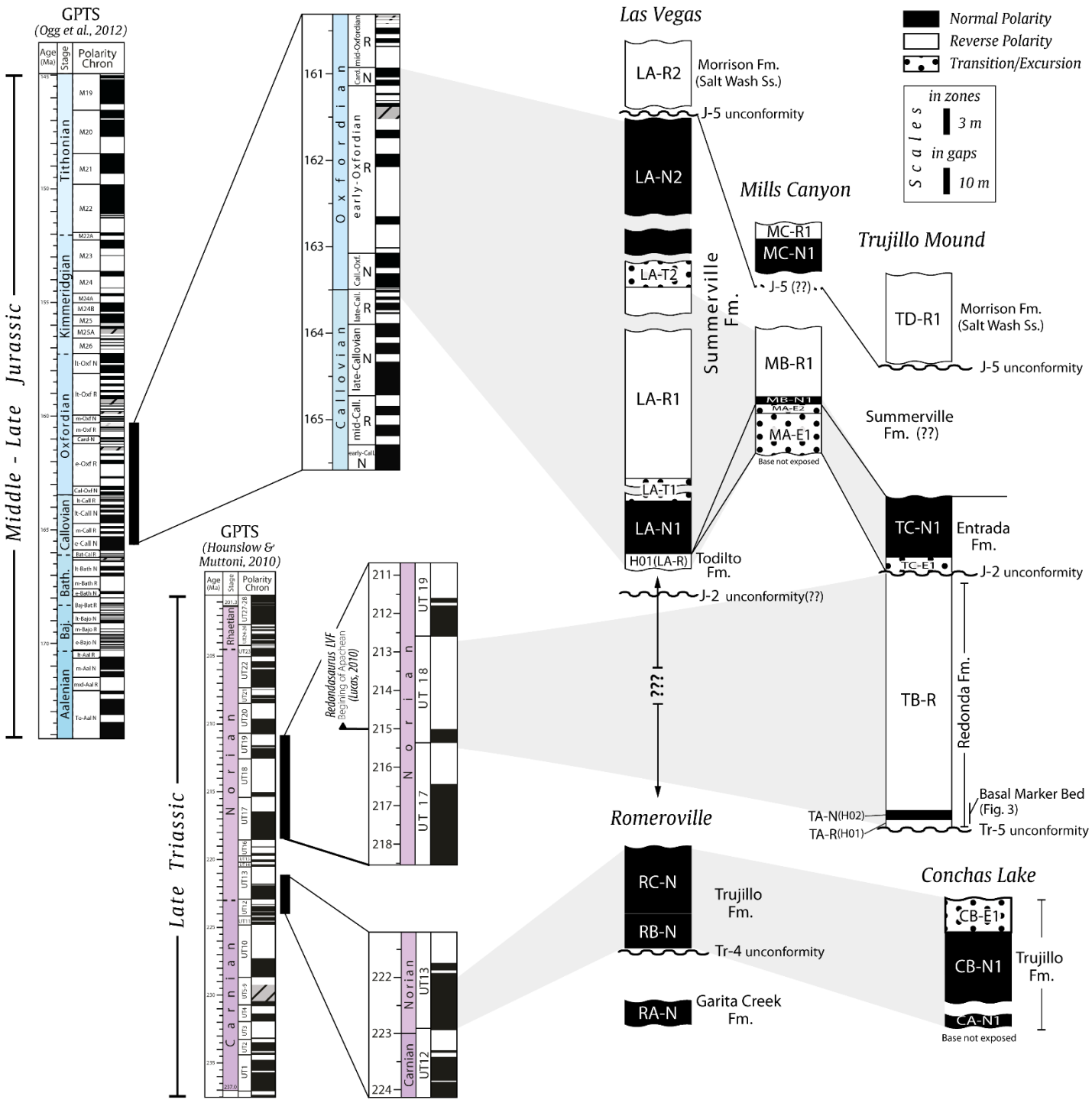

Fig. 11: Proposed magnetic polarity chronology (left) and magnetostratigraphic (right) correlations for Upper Triassic and Middle Jurassic units of east-central New Mexico. GPTS is geomagnetic polarity time scale.

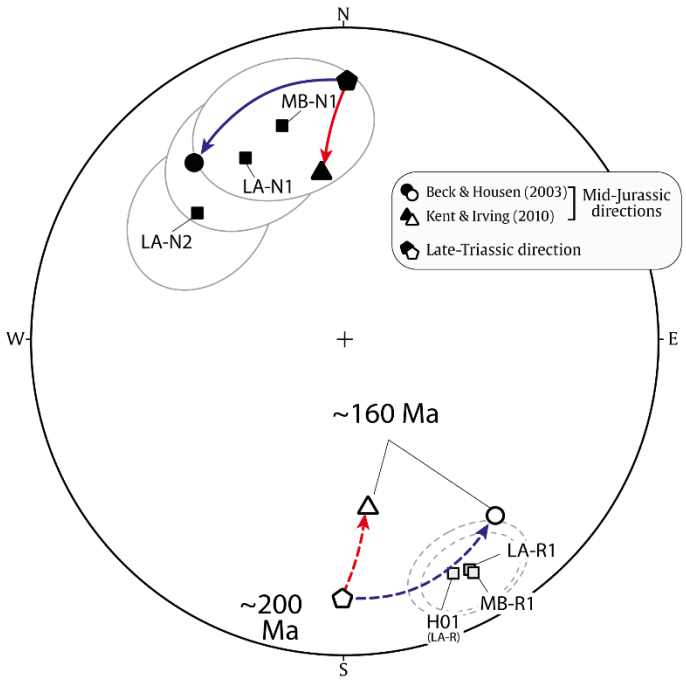

Fig. 12: Equal-area plot of change in directions during late Triassic – Middle Jurassic times calculated from two contradictory apparent polar wander paths (APWP) of North America for coordinates of Middle Jurassic Formations of this study (35.733 N, 255.234 E). The Summerville Formation zone-mean directions plot on the Beck and Housen (2003) expected trend, which validates the lower latitude APWP for North America (e.g. Gordon et al., 1984; May and Butler, 1986), and also confirms a magnetization age of ca.163 Ma for this Formation.

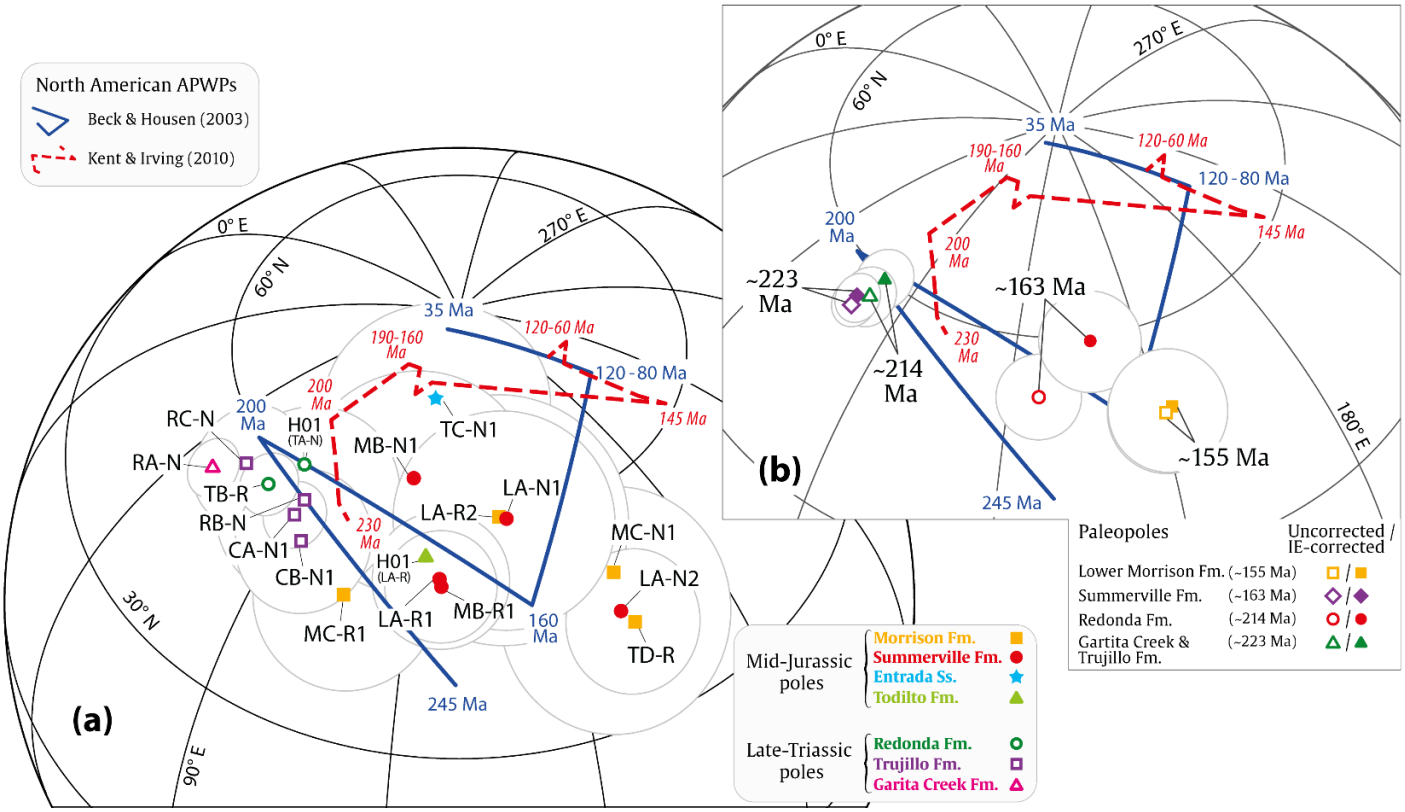

Fig. 13: a) Virtual geomagnetic poles (VGPs) of Upper Triassic and Middle Jurassic zones of east-central New Mexico. b) Uncorrected (open) and IE-corrected(solid) paleomagnetic poles of well-sampled formations of the study area (see Table 4 for more information). Circles are A95 confidence limits about the poles (>20° are not drawn), which are indirectly calculated using Cox's (1970) method.

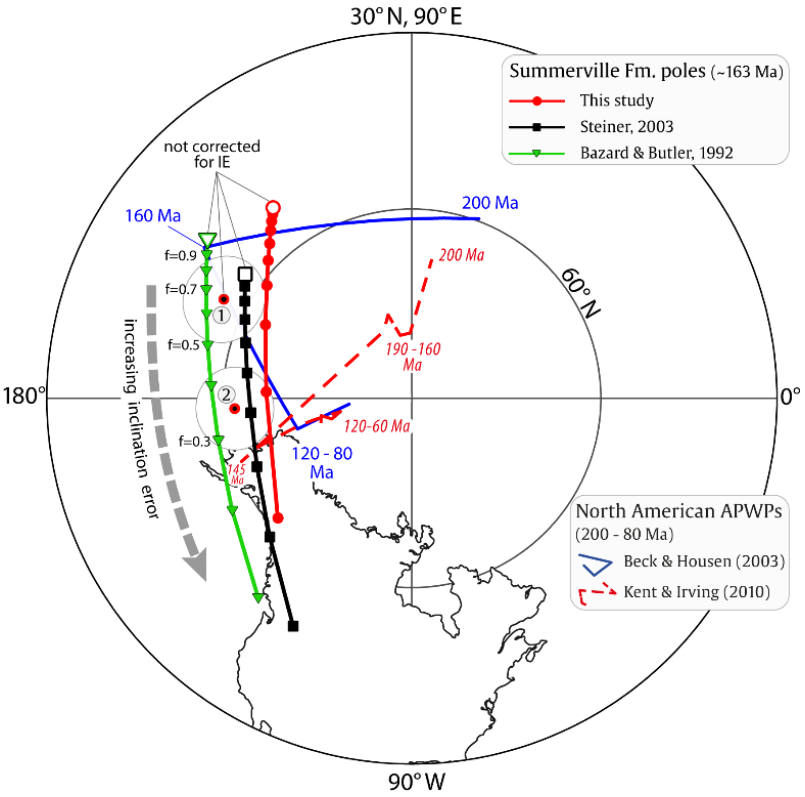

▶ **Fig. 14:** Paleomagnetic poles of Summerville Formation and their simulated paths for inclination error (IE) corrections using King's (1955) equation and a range of flattening factor(*f*) of 0.9 to 0.1. Triangle is Bazard and Butler (1992) pass C sites of Colorado Plateau's Summerville Formation; the square is the group I cratonic pole of Steiner (2003), and the circle is this study's pole calculated from reversed sites (LA-R1, and MBR1). 1: Combined Summerville Formation paleopole, calculated from sample-level line fits of this study and all sample-level directions of Steiner's (2003) Trujillo section; 2: Pole position of (1) corrected for inclination error (IE) using E/I method of Tauxe and Kent (2004). See Fig 10 and Table 3 for more information. This shows that IE correction cannot bring two conflicting APWPs into agreement as suggested by some researches (e.g. Kent and Irving, 2010).

9. Works Cited

Anderson, O.J., Lucas, S.G., 1996. Stratigraphy and depositional environments of Middle and Upper Jurassic rocks, southeastern San Juan basin, New Mexico, in: Goff, F., Kues, B.S., Rogers, M.A., McFadden, L.D., Gardner, J.N. (Eds.), Jemez Mountains Region. New Mexico Geological Society, Guidebook, 47th Field Conference, pp. 205–210.

Anderson, O.J., Lucas, S.G., 1992. The Middle Jurassic Summerville Formation, northern New Mexico. New Mexico Geology 14, 79–92.

Bazard, D., Butler, R., 1992. Paleomagnetism of the Middle Jurassic Summerville Formation, East Central Utah. Journal of Geophysical Research 97, 4377–4385. https://doi.org/10.1029/91JB03071

Beck, M.E., Housen, B.A., 2003. Absolute velocity of North America during the Mesozoic from paleomagnetic data. Tectonophysics, Geodynamic Applications of Palaeomagnetism 377, 33–54. https://doi.org/10.1016/j.tecto.2003.08.018

Biggin, A.J., van Hinsbergen, D.J.J., Langereis, C.G., Straathof, G.B., Deenen, M.H.L., 2008. Geomagnetic secular variation in the Cretaceous Normal Superchron and in the Jurassic. Physics of the Earth and Planetary Interiors, Palaeomagnetism and the Earth's Deep Interior 169, 3–19. https://doi.org/10.1016/j.pepi.2008.07.004

DeCelles, P.G., 2004. Late Jurassic to Eocene evolution of the Cordilleran thrust belt and foreland basin system, western U.S.A. American Journal of Science 304, 105–168. https://doi.org/10.2475/ajs.304.2.105

Deenen, M.H.L., Langereis, C.G., van Hinsbergen, D.J.J., Biggin, A.J., 2011. Geomagnetic secular variation and the statistics of palaeomagnetic directions. Geophys J Int 186, 509–520. https://doi.org/10.1111/j.1365-246X.2011.05050.x

Dunlop, D.J., Özdemir, Ö., 2001. Rock Magnetism: Fundamentals and Frontiers. Cambridge University Press.

Fisher, R.A., 1953. Dispersion on a sphere. Proceedings of the Royal Society of London. Series A. Mathematical and Physical Sciences 217, 295–305.

Gordon, R.G., Cox, A., O'Hare, S., 1984. Paleomagnetic Euler poles and the apparent polar wander and absolute motion of North America since the Carboniferous. Tectonics 3, 499–537. https://doi.org/10.1029/TC003i005p00499

Hagstrum, J.T., 1993. North American Jurassic APW: The current dilemma. Eos Trans. AGU 74, 65–69. https://doi.org/10.1029/93EO00085

Hester, P.C., Lucas, S.G., 2001. Lacustrine depositional environments of the Upper Triassic Redonda Formation, East-Central New Mexico, in: Lucas, S.G., Ulmer-Scholle, D.S. (Eds.), Geology of the Llano Estacado. New Mexico Geological Society, Guidebook, 52nd Field Conference, pp. 153–168.

Hounslow, M.W., 2006. Palaeomag Tools: A tool for analysis of directional data. University of Lancaster.

Hounslow, M.W., Muttoni, G., 2010. The geomagnetic polarity timescale for the Triassic: linkage to stage boundary definitions. Geological Society, London, Special Publications 334, 61–102. https://doi.org/10.1144/SP334.4

Imlay, R.W., 1980. Jurassic paleobiogeography of the conterminous United States in its continental setting (USGS Numbered Series No. 1062), Professional Paper. U.S. Govt. Print. Off.,.

Jackson, M.J., Banerjee, S.K., Marvin, J.A., Lu, R., Gruber, W., 1991. Detrital remanence, inclination errors, and anhysteretic remanence anisotropy: quantitative model and experimental results. Geophys. J. Int. 104, 95–103. https://doi.org/10.1111/j.1365-246X.1991.tb02496.x

Jiang, Z., Liu, Q., Dekkers, M.J., Tauxe, L., Qin, H., Barrón, V., Torrent, J., 2015. Acquisition of chemical remanent magnetization during experimental ferrihydrite–hematite conversion in Earth-like magnetic field—implications for paleomagnetic studies of red beds. Earth and Planetary Science Letters 428, 1–10. https://doi.org/10.1016/j.epsl.2015.07.024

Johnson, R.B., 1974. Geologic map of the Apache Springs quadrangle, San Miguel County, New Mexico (USGS Numbered Series), Geologic Quadrangle. https://doi.org/10.3133/gq1163

Kelley, V.C., 1972. Triassic rocks of the Santa Rosa county, in: Kelley, V.C., Trauger, F.D. (Eds.), East-Central New Mexico. New Mexico Geological Society, Guidebook, 23rd Field Conference, pp. 84–90.

Kent, D.V., Irving, E., 2010. Influence of inclination error in sedimentary rocks on the Triassic and Jurassic apparent pole wander path for North America and implications for Cordilleran tectonics. J. Geophys. Res. 115, B10103. https://doi.org/10.1029/2009JB007205

Kent, D.V., Kjarsgaard, B.A., Gee, J.S., Muttoni, G., Heaman, L.M., 2015. Tracking the Late Jurassic apparent (or true) polar shift in U-Pb-dated kimberlites from cratonic North America (Superior Province of Canada). Geochem. Geophys. Geosyst. 16, 983–994. https://doi.org/10.1002/2015GC005734

Kent, D.V., Tauxe, L., 2005. Corrected Late Triassic Latitudes for Continents Adjacent to the North Atlantic. Science 307, 240–244. https://doi.org/10.1126/science.1105826

King, R.F., 1955. The Remanent Magnetism of Artificially Deposited Sediments. Geophys Suppl MNRAS 7, 115–134. https://doi.org/10.1111/j.1365-246X.1955.tb06558.x

Kirschvink, J.L., 1980. The least-squares line and plane and the analysis of palaeomagnetic data. Geophys. J. Int. 62, 699–718. https://doi.org/10.1111/j.1365-246X.1980.tb02601.x

Kruiver, P.P., Dekkers, M.J., Heslop, D., 2001. Quantification of magnetic coercivity components by the analysis of acquisition curves of isothermal remanent magnetisation.

Earth and Planetary Science Letters 189, 269–276. https://doi.org/10.1016/S0012-821X(01)00367-3

Lucas, S.G., 2018. The Upper Jurassic Morrison Formation in north-central New Mexico–Linking Colorado Plateau stratigraphy to the stratigraphy of the High Plains. Geology of the Intermountain West 5, 117–129. https://doi.org/10.31711/giw.v5i0.23

Lucas, S.G., 2010. The Triassic timescale based on nonmarine tetrapod biostratigraphy and biochronology. Geological Society, London, Special Publications 334, 447–500. https://doi.org/10.1144/SP334.15

Lucas, S.G., 2004. The Triassic and Jurassic systems in New Mexico, in: Mack, G.H., Giles, K.A. (Eds.), The Geology of New Mexico: A Geologic History. New Mexico Geological Society Special Publication, pp. 137–152.

Lucas, S.G., 1995. Triassic stratigraphy and chronology in New Mexico. New Mexico Geology 17, 8–17.

Lucas, S.G., Anderson, O.J., 1998. Jurassic stratigraphy and correlation in New Mexico. New Mexico Geology 20, 97–104.

Lucas, S.G., Anderson, O.J., 1997. The Jurassic San Rafael Group, Four Corners region, in: Anderson, O.J., Kues, B.S., Lucas, S.G. (Eds.), Mesozoic Geology and Paleontology of the Four Corners Region. New Mexico Geological Society, Guidebook, 48th Field Conference, pp. 115–132.

Lucas, S.G., Estep, J.W., Anderson, O.J., 1999. Correlation of Jurassic strata from the Colorado Plateau to the High Plains, across the Rio Grande rift, north-central New Mexico, in: Pazzaglia, F.J., Lucas, S.G. (Eds.), Albuquerque Geology. New Mexico Geological Society, Guidebook, 50th Field Conference, pp. 317–326.

Lucas, S.G., Heckert, A.B., Hunt, A.P., 2001. Triassic stratigraphy, biostratigraphy and correlation in east-central New Mexico, in: Lucas, S.G., Ulmer-Scholle, D.S. (Eds.), Geology of the Llano Estacado. New Mexico Geological Society, Guidebook, 52nd Field Conference, pp. 85–102.

Lucas, S.G., Hunt, A.P., 1993. Tetrapod biochronology of the Chinle Group. New Mexico Museum of Natural History and Science Bulletin 3, 327–329.

Lucas, S.G., Hunt, A.P., 1989. Revised Triassic stratigraphy in the Tucumcari basin. Dawn of the Age of Dinosaurs in the American Southwest 150.

Lucas, S.G., Spielmann, J.A., 2013. Magnetostratigraphy of the Upper Triassic Chinle Group in New Mexico: An appraisal of 40 years of analysis. New Mexico Museum of Natural History and Science Bulletin 61, 375–381.

Lucas, S.G., Woodward, L.A., 2001. Jurassic strata in east-central New Mexico and their regional significance, in: Lucas, S.G., Ulmer-Scholle, D.S. (Eds.), Geology of the Llano

Estacado. New Mexico Geological Society, Guidebook, 52nd Field Conference, pp. 203–212.

Lurcock, P.C., Wilson, G.S., 2012. PuffinPlot: A versatile, user-friendly program for paleomagnetic analysis: TECHNICAL BRIEF. Geochemistry, Geophysics, Geosystems 13, n/a-n/a. https://doi.org/10.1029/2012GC004098

Mankin, C.J., 1972. Jurassic strata in northeastern New Mexico, in: Kelley, V.C., Trauger, F.D. (Eds.), East-Central New Mexico. New Mexico Geological Society, Guidebook, 23rd Field Conference, pp. 91–97.

May, S.R., Butler, R.F., 1986. North American Jurassic Apparent Polar Wander: Implications for plate motion, paleogeography and Cordilleran tectonics. J. Geophys. Res. 91, 11519–11544. https://doi.org/10.1029/JB091iB11p11519

McFadden, P.L., 1998. The fold test as an analytical tool. Geophysical Journal International 135, 329–338. https://doi.org/10.1046/j.1365-246X.1998.00640.x

McFadden, P.L., McElhinny, M.W., 1988. The combined analysis of remagnetization circles and direct observations in palaeomagnetism. Earth and Planetary Science Letters 87, 161–172. https://doi.org/10.1016/0012-821X(88)90072-6

Ogg, J.G., Hinnov, L.A., Huang, C., 2012. Jurassic, in: The Geologic Time Scale. Elsevier, pp. 731–791. https://doi.org/10.1016/B978-0-444-59425-9.00026-3

Pipiringos, G.N., O'Sullivan, R.B., 1978. Principal unconformities in Triassic and Jurassic rocks, western interior United States; a preliminary survey (USGS Numbered Series No. 1035-A), Professional Paper. United States Government Printing Office, Washington, D. C.

Skotnicki, S.J., 2003. Geologic Map of the Las Vegas Quadrangle, San Miguel County, New Mexico (No. OF-GM 72), Geologic Quadrangle. New Mexico Bureau of Geology & Mineral Resources, New Mexico Institute of Mining & Technology.

Steiner, M.B., 2003. A cratonic Middle Jurassic paleopole: Callovian-Oxfordian stillstand (J-2 cusp), rotation of the Colorado Plateau, and Jurassic North American apparent polar wander. Tectonics 22, 1020. https://doi.org/10.1029/2001TC001284

Steiner, M.B., Lucas, S.G., Shoemaker, E.M., 1994. Correlation and Age of the Upper Jurassic Morrison Formation from Magnetostratigraphic Analysis 315–330.

Tauxe, L., 2010. Essentials of Paleomagnetism. University of California Press.

Tauxe, L., 2005. Inclination flattening and the geocentric axial dipole hypothesis. Earth and Planetary Science Letters 233, 247–261. https://doi.org/10.1016/j.epsl.2005.01.027

Tauxe, L., Kent, D.V., 2004. A Simplified Statistical Model for the Geomagnetic Field and the Detection of Shallow Bias in Paleomagnetic Inclinations: was the Ancient Magnetic Field Dipolar?, in: Channell, J.E.T., Kent, D. V., Lowrie, W., Meert, J.G. (Eds.), Timescales Of The Paleomagnetic Field. American Geophysical Union, pp. 101–115.

Tauxe, L., Kodama, K.P., Kent, D.V., 2008. Testing corrections for paleomagnetic inclination error in sedimentary rocks: A comparative approach. Physics of the Earth and Planetary Interiors, Palaeomagnetism and the Earth's Deep Interior 169, 152–165. https://doi.org/10.1016/j.pepi.2008.05.006

Tauxe, L., Watson, G.S., 1994. The fold test: an eigen analysis approach. Earth and Planetary Science Letters 122, 331–341. https://doi.org/10.1016/0012-821X(94)90006-X

Van Fossen, M.C., Kent, D.V., 1990. High-latitude paleomagnetic poles from Middle Jurassic Plutons and moat volcanics in New England and the controversy regarding Jurassic Apparent Polar Wander for North America. J. Geophys. Res. 95, 17503–17516. https://doi.org/10.1029/JB095iB11p17503

Wanek, A.A., 1962. Reconnaissance geologic map of parts of Harding, San Miguel, and Mora Counties, New Mexico (Report No. 208), Oil and Gas Investigation Map. https://doi.org/10.3133/om208

Wilcox, W.T., Currie, B.S., 2008. Sequence Stratigraphy of the Jurassic Curtis, Summerville, and Stump Formations, Eastern Utah and Northwest Colorado 9–42.

Appendix A

Supplementary table 1: Paleomagnetic directions of Upper Triassic and Middle Jurassic strata from east-central New Mexico, calculated from line fits (using PCA of Kirschvink [1980]) with the maximum angular deviation (MAD) angle <10° on smoothed data (MAD<5° for anchored PCA). *: TB-R zone mean direction without excluding excursion zones; n/N: number of directions used to calculate the zone mean/ total number of specimens, Dec and Inc: tilt-corrected declination and inclination of the characteristic remanent magnetization (ChRM) component; a95 and k: half-angle of the 95% confidence limit and precision parameter of Fisher (1953) statistics; R: length of the resultant vector; lat. (long.): north latitude (east longitude) of the paleopole locations (negative sign indicates south latitude).

Set	Zone	n/N	Mean direction					VGP	
			Dec	Inc	a95	k	R	lat.	long.
Trujillo Mount									
TD	TD-R1	9/41	127.4	-44.1	20.1	7.54	7.94	-44.3	348.3
TC	TC-N1	4/13	354.4	35.9	34.1	8.24	3.64	73.7	94.2
	TC-T1	1/5	3.2	37.4	-	-	-	75.2	63.7
TB	TB-R *	16/112	175.2	1.6	12.7	9.40	14.40	-53.4	263.4
TA	H02 (TA-N)	2/9	357.5	14.1	24.8	103.28	1.99	61.5	80.6
	H01 (TA-R)	5/5	150.6	-57.9	9.5	66.37	4.94	-66.5	1.5
Mills Canyon									
MC	MC-R1	1/9	152.2	13.2	-	-	-	-40.0	292.9
	MC-N1	5/7	314.9	41.9	27.8	8.50	4.53	49.6	161.6
MB	MB-R1	4/26	154.8	-16.3	8.3	122.27	3.98	-54.1	301.6
	MB-N1	2/5	342.5	23.0	44.0	34.28	1.97	61.3	113.4
MA	MA-E2	1/5	250.2	30.9	-	-	-	-5.5	190.8
	MA-E1	2/13	161.4	-24.7	64.1	17.36	1.94	-61.6	296.5
Las Vegas									
LA	LA-R2	1/6	150.7	-54.0	-	-	-	-66.1	351.0
	LA-N2	2/22	286.2	31.7	34.7	53.90	1.98	22.9	170.0
	LA-T2	1/6	107.5	-29.1	-	-	-	-23.1	347.9
	LA-R1	8/28	141.0	-19.9	29.6	4.46	6.43	-46.5	319.0
	LA-T1	3/6	289.7	68.9	32.7	15.30	2.87	38.9	207.1
	LA-N1	7/10	337.9	37.9	19.4	10.61	6.43	66.0	134.2
	H01 (LA)	-/3	-	-	-	-	-	-	-
Romeroville exit									
RC	RC-N	11/58	7.6	8.9	21.1	5.66	9.23	58.2	60.3
RB	RB-N	8/26	354.4	4.9	21.4	7.64	7.08	56.5	84.9
RA	RA-N	15/64	3.9	-2.3	7.8	25.00	14.44	53.1	68.2
Conchas Lake									
CB	CB-E1	-/17	-	-	-	-	-	-	-
	CB-N1	6/35	344.6	-6.8	28.0	6.67	5.25	48.7	99.4
CA	CA-N1	6/18	353.1	4.7	9.3	52.35	5.90	56.4	88.3

Supplementary table 2: Paleomagnetic directions of Upper Triassic and Middle Jurassic strata from east-central New Mexico, calculated from line and great-circle with the maximum angular deviation (MAD) angle <10° on smoothed data. L/GC: number of line fits (principal component analysis (PCA) of Kirschvink [1980]) / great-circle fits to calculate the mean (McFadden and McElhinny, 1988). See Supplementary Table 1 for more information.

Set	Zone	n/N	L /GC	Mean direction					VGP	
				Dec	Inc	a95	k	R	lat.	long.
Trujillo Mount										
TD	TD-R1	9/41	9/-	127.4	-44.1	20.1	7.54	7.94	-44.3	348.3
TC	TC-N1	4/13	4/-	354.4	35.9	34.1	8.24	3.64	73.7	94.2
	TC-T1	1/5	1/-	3.2	37.4	-	-	-	75.2	63.7
TB	TB-R *	34/112	16/18	174.6	-4.7	9.3	7.83	30.94	-56.5	265.1
TA	H02 (TA-N)	3/9	2/1	355.4	14.1	13.7	112.95	2.99	61.3	84.8
	H01 (TA-R)	5/5	5/-	150.6	-57.9	9.5	66.37	4.94	-66.5	1.5
Mills Canyon										
MC	MC-R1	1/9	1/-	152.2	13.2	-	-	-	-40.0	292.9
	MC-N1	5/7	5/-	314.9	41.9	27.8	8.50	4.53	49.6	161.6
MB	MB-R1	10/26	4/6	149.7	-21.5	16.9	9.60	9.38	-53.1	311.2
	MB-N1	2/5	2/-	342.5	23.0	44.0	34.28	1.97	61.3	113.4
MA	MA-E2	1/5	1/-	250.2	30.9	-	-	-	-5.5	190.8
	MA-E1	3/13	2/1	162.0	-21.4	31.4	22.19	2.93	-60.3	293.3
Las Vegas										
	LA-R2	4/6	1/3	142.5	-46.6	17.4	52.78	3.97	-57.4	341.9
	LA-N2	2/22	2/-	286.2	31.7	34.7	53.90	1.98	22.9	170.0
	LA-T2	3/6	1/2	91.9	-43.2	62.7	12.04	2.92	-15.7	4.7
	LA-R1	12/28	8/4	143.2	-17.4	20.7	5.35	10.32	-47.2	315.4
	LA-T1	3/6	3/-	289.7	68.9	32.7	15.30	2.87	38.9	207.1
LA	LA-N1	7/10	7/-	337.9	37.9	19.4	10.61	6.43	66.0	134.2
	H01 (LA)	-/3	-/-	-	-	-	-	-	-	-
Romeroville exit										
RC	RC-N	11/58	-/-	7.6	8.9	21.1	5.66	9.23	58.2	60.3
RB	RB-N	8/26	-/-	354.4	4.9	21.4	7.64	7.08	56.5	84.9
RA	RA-N	15/64	-/-	3.9	-2.3	7.8	25.00	14.44	53.1	68.2
Conchas Lake										
CB	CB-E1	3/17	-/3	215.9	-70.7	-	6.78	2.93	-58.5	115.9
	CB-N1	7/35	6/1	345.2	-4.8	24.5	7.12	6.23	49.8	99.0
CA	CA-N1	6/18	-/-	353.1	4.7	9.3	52.35	5.90	56.4	88.3